Phenomenological Modeling of The Nucleated Polymerization of Human Islet Amyloid Polypeptide; a Combined Experimental and Theoretical Approach

by

James Bailey

B.Sc., Appalachian State University, 2005

A THESIS SUBMITTED IN PARTIAL FULFILLMENT OF THE REQUIREMENTS FOR THE DEGREE OF

MASTER OF SCIENCE

in

THE FACULTY OF GRADUATE STUDIES

(Mathematics)

THE UNIVERSITY OF BRITISH COLUMBIA

(Vancouver)

April 2008

©James Bailey

Abstract

The inverse scattering problem is based on the scattering theory in physics, where measured data such as radiation from an object is used to determine the unique structure of the object in question. This approach has been widely successful in fields ranging from geophysics and medical imaging, to quantum field theory.

In 1996 Henrik Flyvbjerg suggested that a similar approach could be used to study a reaction far from equilibrium of the self-assembly of a nucleation dependent biopolymer and, under certain conditions, uniquely determine the kinetics of the assembly. Here we use this approach to elucidate the unique structure of human islet amyloid polypeptide, also known as amylin, *in-vitro*.

We use a systematic phenomenological analysis of the amount of monomer in fibril, of amylin, for various initial concentrations from an unstructured monomer pool. Using the assumption that nucleation is the rate-limiting step in fibril formation, we invoke mass action to develop our model. We find that the fibrillogenesis of amylin is well described by a nucleation dependent polymerization event that is characteristic of the sigmoidal shape of the reaction profile generated by our data. Furthermore, we find a second nucleation event is needed to accurately match model predictions to the observed data for the kinetic profiles of fibril formation, and the experimental length distributions of mature fibrils from *in-vitro* assays.

This analysis allows for the theoretical determination of each step of assembly in the nucleation process. Specifically, we find the number of steps to nucleation, the size of each oligomer formed in the nucleation process, the nucleus size, and the elongation kinetics of fibrils. The secondary nucleation process is found to be a fibril dependent surface mediated nucleation event and is similar in reaction order to the primary nucleation step. Model predictions are found to be congruent with experimental assay results of oligomer populations and monomer concentration. We demonstrates that, a persistent oligomer formation is a natural and necessary consequence of nucleated fibril formation, given certain qualitative features of the kinetic profile of fibril formation. Furthermore, the modeling assumptions about monomer and fibril mass are in agreement with experiment.

Contents

List of Figures

.

Acknowledgments

The procedure used here to elucidate the kinetic steps in the formation of human islet amyloid polypeptide fibrils was first suggested by Henrik Flyvbjerg in 1996 in a case study of microtubule dynamics. While the model of amyloid fibrillogenes presented here is an extension of this work, it finds its foundation in the work preformed by Flyvbjerg. I am indebted to Dr. Leah Keshet for the suggestion to model amyloid in this manner, and to Dr. Daniel Coombs for first exposing me to the fascinating procedure outlined by Flyvbjerg. Furthermore, Dr. Keshet has proven invaluable in the formation of this thesis. I would also like to acknowledge Dr. Bruce Verchere and Kate Potter, a MD/PHD student in Vercher's lab at the Childrens' Hospital, for giving me my introduction to the assays I have used to produce the data outlined in this thesis. Funding for this research has been provided by MITACS, the BC Childrens' and Women's Hospital, and the University of British Columbia. I would also like to acknowledge Dr. Das Raibatak for his insights and my introduction to Mathmatica.

1 Introduction

1.1 Phenomenological Modeling of The Nucleated Polymerization of Human Islet Amyloid Polypeptide; a Combined Experimental and Theoretical Approach

The presence of amyloid deposits is indicative of the diseased state in many degenerative disorders. Normally soluble precursor proteins form deposits as oligomers and amyloid fibrils which amalgamate to form plaques. These fibrilary tangles and associated oligomers are thought to be responsible for decreased cellular function and cytotoxicity (toxic cell death). Kinetic profiles of amyloid fibril formation, *in-vitro*, reveal a stereotypical sigmoid shape. This kinetic profile is characteristic of nucleated polymerization. However, the profile generated by amyloid fibrils shows a pronounced lag phase, followed by an abrupt formation of fibrils which does not readily fit current nucleation polymerization models. Here we review several models proposed for the nucleated polymerization of amyloid fibril formation and demonstrate their inability to accurately describe the formation of fibrillogenesis for human islet amyloid polypeptide (hIAPP) *in-vitro*. We then outline a generic procedure for determining the kinetic steps of amyloid fibril assembly, which exploits the observation that kinetic profiles for various initial concentrations of hIAPP may be rescaled by their initial precursor protein concentration and characteristic time to completion, resulting in approximant collapse of data to a single kinetic profile. This property of hIAPP, and likely other amyloid fibril formation kinetics, allows for the complete theoretical determination of the kinetics of assembly of hIAPP *in-vitro*. Here we have determined that hIAPP fibrils are assembled through a primary nucleation event and facilitated by a rapid secondary nucleation event that is fibril dependent. As a bonus, the analysis predicts the formation of oligomers as a natural consequence of fibril formation and describes their lifetimes. Thus, we have elucidated not only the complete kinetics of formation of fibrils but also shown how this process leads to a persistent oligomer population. The model presented here may serves as a predictive tool allowing researchers to "see" the effects of altering formation kinetics at specific steps of fibril and oligomers populations. The procedure we demonstrate is readily applicable to any nucleated polymerization event that exhibits collapsible kinetic data under systematic scaling.

Models of nucleated polymerization have been widely successful in describing the assembly kinetics of many self-assembling polymers such as actin (1,2) and microtubules (3,4). The kinetic profiles of these polymerization events exhibit a distinct lag phase where little to no polymer is formed, followed by an abrupt growth phase where polymerization occurs rapidly. This process results in a sigmoidal curve representing the mass of monomers in polymer form over time. However, single nucleated polymerization alone is inadequate to describe the kinetics of amyloid fibril formation due to the rapid rise time observed in *in-vitro* experiments. Specifically, in hIAPP, the rise time for polymerization

is considerably shorter than the lag phase. The observed time scale of the rise time relative to the lag phase in hIAPP and other amyloid fibrils suggest a secondary means of fibril tip formation, on which fibrils may grow and elongate. Several models have been suggested to describe this process. Notably, branching, fibril breaking and fibril dependant nucleation have all been proposed as mechanisms for secondary nucleation of fibril growth (5,6,7). Despite these modeling attempts, the nature of fibril formation in amyloid disease is poorly understood. The necessity for understanding the kinetics of assembly is relevant not only to the physical chemistry of amyloid fibril formation but also to the pathology of amyloidosis as well. Nucleation rates, specifically secondary nucleation process, may be drastically altered by environmental factors and may contribute to the pathology of the disease (6).

Recent cell toxicity assays suggest that the oligomeric species found alongside growing and mature fibrils may be the primary cause of cell toxicity in hIAPP fibrillogenesis. Much work has been done to describe an alternate pathway for oligomer construction which competes and is distinct from fibrillogenesis. Here we show that persistent oligomer populations are a natural consequence of fibril formation in hIAPP and we give a global analysis for their time course, size in monomeric units and relative abundance. In this analysis we use scaling properties of hIAPP kinetic data to elucidate the exact steps involved in primary and secondary nucleation. The modeling procedure utilized here allows the data to determine the type of secondary nucleation that most naturally fits the kinetic profile observed and makes definite predictions about length distributions of hIAPP fibrils. These predictions are in agreement with observation. Furthermore, the analysis of the data reveals a natural source of potentially toxic oligomer species and predicts time courses for their assembly and lifetimes. These predicted time courses are shown to be congruent with experimental observation.

1.2 Amyloidosis

Amyloidosis is the diseased state associated with abnormal, insoluble, amyloid deposits in organs and tissue. Insoluble amyloid deposits from normally soluble precursor proteins in the form of oligomers, fibrils, and amyloid plaques are pathogenic features in many known diseases. Numerous species of amyloid deposits are known to exist, stemming from over 20 categorical precursor proteins (8,9,10). The presence of these deposits may be classified into two groups of amyloidosis, systematic and localized (8).

Systematic amyloidosis encompasses diseases where precursor proteins circulate through an organ or system. For example, chronic inflammation associated with N-terminal fragment deposits in rheumatoid arthritis and tuberculosis is driven by acute phase serum amyloid proteins, a class of apolipoproteins. These apolipoproteins are secreted during

acute inflammation by the liver and circulate to the site of inflammation. Other common examples of systemic amyloid precursor producers include the heart and kidneys. Localized amyloidosis, describes the deposition of amyloid in a target organ where the production of the precursor protein is created on-site in the organ. Examples include Alzheimer's disease and type II diabetes where amalgamations of fibrous deposits are indicative of the diseased state. In Alzheimers disease, amyloid-β (Aβ) is known to accumulate in the cerebrovascular and cortical regions (11,12,13). In type II diabetes, islet amyloid polypeptide (IAPP) fibrils aggregate in plaques in the extracellular regions surrounding pancreatic islets. Both animal studies which show, amyloid deposits in the islets before the onset of hypoglycemia and abnormally low blood sugar levels, and *in-vitro* studies, which show the formation and presence of IAPP fibrils are cytotoxic, imply that amyloid deposition plays a causative role in type II diabetes. Despite this evidence of causality and the well documented nature of amyloid deposits, the kinetics of formation of these deposits is largely unknown.

1.3 Islet Amyloid Polypeptide

1.3.1 Secretion of IAPP Mirrors That of Insulin

IAPP is a precursor protein that is co-secreted with insulin by the pancreatic β-cell islets. The accumulation of islet amyloid in the extracellular space between islets is indicative of type II diabetes and is present in nearly all instances of the disease. Though discovered over a century ago (14), the insoluble nature of islet amyloid posed serious impairments to the isolation and analysis of its components until the late 1980's when Westermark and others (15,16,17) successfully isolated and identified the unique amino acid sequence for the precursor protein IAPP, also known as amylin.

Secretion levels of hIAPP have been correlated with insulin secretion levels as related to nutritional stimuli (18-22). Fasting mice assays report IAPP/insulin ratios of $1/10 - 1/6$ (23,24). However, the clearance rates of insulin and IAPP are dissimilar in the plasma. IAPP, like C Peptide, the peptide created when pro insulin is split into insulin and C-peptide, is cleared by the kidneys. In contrast, insulin clearance is a complex process involving the liver, kidney, and muscle as major participants (25) This variation in clearance rates, as well as recorded IAPP plasma levels following stimulation of β-cells for peptide release with glucose or non glucose response suggest a physiological ratio of IAPP to insulin closer to 1/100 (23,26,27,28). This level is in good agreement with *in-vitro* experimental observations (29). Furthermore, IAPP levels have been shown to mirror the secretion of insulin in humans, and factors regulating insulin levels have also been shown to regulate IAPP levels (8). Specifically, insulin sensitivity as associated with type II diabetes has been shown to affect secretion of IAPP from islets (26,27). Notable experimental evidence indicates increased levels of IAPP in populations of obese individuals (21,23,24).

A similar study shows increased levels of IAPP mirror increased levels of insulin in pregnant women (30). This correlation of IAPP secretion with insulin secretion is also noted in pathologies associated with depleted insulin levels, such as β-cell function depletion associated with type I and II diabetes(19,20,22,27,31,32,33). Individuals with diminished glucose to,lerance associated with type II diabetes, as well as family members of individuals with the disease show retarded release of IAPP to oral glucose intake(22,27,31). Despite the detailed analysis of the secretion and co-production of IAPP, and the implications of a causative role in type II diabetes, little is known about the normal biological function of the peptide.

1.3.2 Physiological Function of Islet Amyloid Polypeptide

IAPP has been implicated in insulin regulation, both in the impediment of insulin secretion with glucose stimulation (34,35,36) and suppression of insulin mediated glucose uptake, specifically in skeletal muscles (37,38). Furthermore, *in-vitro* studies of isolated islets show a decrease in the production of glycogen, a short term sugar storage structure. However, these studies used inordinately high levels of IAPP and were not altogether reproducible. Nevertheless, experiments with IAPP deficient mice exhibit enhanced insulin secretion and glycogen clearance rates.

Intriguingly, IAPP has been correlated with food intake and weight control. Injections of an IAPP antagonist into the circulatory system of the brain has been demonstrated to show increases in caloric intake and body mass in rats (39-42). Other physiological functions implied for IAPP are regulation of renal function (43,44), and calcium homeostasis (45,46).

2 Cytotoxicity of Islet Amyloid

In non-diseased individuals, IAPP secreted with insulin by β-cells is maintained in the well regulated intracellular environment. In this environment, IAPP is maintained in a monomeric form and processed normally. Islet transplant studies with mice suggest the initiation of fibril formation may occur intracellularly with the mis-processing of (pro)IAPP (47,48). This mis-processed (pro)IAPP remains inert while in the intracellular region. Once secreted into the intercellular fluid, this malformed IAPP would be exposed to aggravating levels of pH and calcium. Similar perturbations in pH and calcium levels have been shown to facilitate the self assembly of IAPP fibrils *in-vitro* (49,50,51). Furthermore, heparin sulfate proteoglycans and other compounds found in mature amyloid deposits are readily accessible in this extracellular fluid. *In-vitro* assays with thioflavin-T demonstrate heparin accelerates the formation of IAPP fibrils with similar pH levels (52), Section [7.4.1]. Taken together, these observations suggest an extracellular environment highly favorable for the production of toxic amyloid deposits of IAPP.

2.1 Fibril Toxicity

Many studies support the theory of fibril cytotoxicity. Indeed, the almost universal observation of IAPP fibrils in autopsy studies of chronic diabetics gives superficial evidence of their toxicity. Supporting *in-vitro* studies have shown IAPP fibrils to be cytotoxic in β-cell cultures (34,35). Despite this body of evidence for fibril toxicity, several studies have shown that increased fibril formation does not increase cell death. This avenue of research has opened the door to an alternate explanation for the cytotoxicity of IAPP deposits, namely oligomeric species that may represent either early stages in fibril development (8,35) or a distinct pathway of oligomer formation(36).

2.2 Oligomer Toxicity

Oligomeric species of IAPP have been noted alongside both growing and mature fibrils (53), Section [5.3]. These oligomers have been implicated as the cytotoxic component of amyloid formation (53,54), Section [5.5]. However, the nature of formation of these species is currently the subject of much debate. Models have been proposed that imply that the oligomers are a disperse phase balanced by the presence of IAPP monomers (55). This theory evolved to account for the lack of concentration-dependence in IAPP fibril formation as measured by anisotropy assays. Other studies have suggested that oligomer formation is a process distinct from and competitive with fibril formation (36). This model suggests that the persistent nature of oligomers, well beyond the formation phase of fibrils, supports a distinct pathway for the formation of oligomers. In this thesis, a theory for nucleated fibrillogenesis of IAPP is presented which demonstrates that persistent oligomer formation is a natural and necessary consequence of nucleated fibril formation, given certain qualitative features of the kinetic profile of fibril formation.

2.3 Need For a Unified Model

Given the contradictory evidence for fibril toxicity cited above and the growing body of evidence of the role of oligomeric cytotoxicity, an exact understanding of fibrillogenesis of IAPP is needed to predict the potential effects of inhibitors on not only fibril populations, but oligomer populations as well. It is the intent of this thesis to help elucidate the underlying kinetics of IAPP fibrillogenesis and, thereby, help to clarify conflicting observations found in the literature. Furthermore, a unique kinetic description for the self assembly of amyloid fibrils and their associated oligomers may help in the search for potential therapies for the early detection and control of type II diabetes.

3 Experimental Methods

Historically, the "starch-like" appearance of fibrous deposits found in diseased tissue were termed amyloid by Virchow in 1855, after observing blue staining of acid-treated fibrils by iodine. This staining is now known to be due to the protein present in these fibril deposits. Several compounds have been shown, under appropriate conditions, to selectively stain amyloid deposits. The histological benzothiazole dyes thioflavin S (Th-S) and thioflavin T (Th-T) along with the diazobenzide sulfate dye, and Congo red were found to stain amyloid in a number of pathological settings (56). Furthermore, several other fluorescent and non fluorescent dyes including Phorwhite BBU and Sirus Red share this property.

Th-S, a mentholated, sulfonated polymerized primulin preparation with an uncharacterized structure, is commonly used for histological demonstrations of amyloid fibrils where long wavelength UV excitation can be used. The enhanced emission intensity observed by the binding of Th-S to amyloid fibrils exhibits a magnification of several fold, while the emission spectra is unaltered. This characteristic excitation of TH-S results in high background levels of fluorescence in solution and renders TH-S unsuited for quantitative analysis in solution(56).

Th-T however, exhibits a notable spectral shift, without enhanced emission intensity, when bound to amyloid fibrils but not monomers or β-sheet conformations (56). The specificity with which Th-T exhibits fluorescence shift when bound to amyloid fibrils forms the basis for assays using Th-T fluorescence shift as a measure of monomer mass in fibril form.

3.1 Thioflavin T

The characteristic behavior of Th-T of exhibiting a fluorescence spectral shift without altering emissions spectrum implies Th-T's 115-nm red shift in fluorescence is associated with a change in the ground state energy upon binding to amyloid fibrils, and does not result from changes in the excitation state energies. The later is implied by a shift in the emission spectrum (56). Regardless of these observations, the nature of the observed behavior of the Th-T amyloid fibril complex remains to be elucidated.

The unknown nature of the amyloid fibril Th-T complex makes exact quantification of the relationship between fluorescence and amyloid fibril all but impossible to obtain. Nevertheless, the consistency in fluorescence shift associated with the complex is useful for determining relative amounts of amyloid fibril formed over time, as well as relative rates of fibril formation for various initial concentrations of IAPP monomer. Fortunately, relative rates of fibril formation for various initial monomer concentrations is all that is required, in the case of hIAPP, to determine the unique kinetics of assembly in fibrillo-

genesis. Given these considerations, this thesis utilizes a Th-T assay as described in the Materials and Methods section as a basis for modeling hIAPP fibrillogenesis.

3.2 Dot Blots

Western Blot assays have been traditionally used to determine the presence of specific proteins in a sample. Gel electrophoresis is used to segregate proteins in the sample; these proteins are then exposed to antibodies specific to the protein under scrutiny and examined for interactions. Recently, Dot Blot assays have replaced Western, Southern, and Northern Blot assays in a number of studies. The Dot Blot assay has the advantage of not requiring gel electrophoresis or the complex blotting procedures associated with the other assays. However, Dot Blots give no information about the size of the protein present. This thesis reports results from Dot Blot assays used to establish the time order of formation and corresponding lifetimes of oligomers during and after fibril formation of IAPP, as described in the Materials and Methods section.

3.3 Cell Toxicity

Cultured β-cells were exposed to various initial concentrations of hIAPP and were screened for viability over time by measuring cellular metabolism. These assays give a rough estimate of when toxicity began and help elucidate any dependence of cytotoxicity on initial IAPP monomer concentration.

3.4 Solubility Assay

To test for monomer and soluble oligomer over time a filtration assay was utilized. This assay tracks the soluble monomer and small soluble oligomer present in solution over time. The assay was used as confirmation of the assumption presented in this thesis model that all monomers are consumed as fibril formation ceases, corresponding with a plateau in Th-T fluorescence. Furthermore, this assay allows for the quantitative tracking of soluble monomers and small soluble oligomers over time. It can be matched to model predictions to help support the theory presented here.

3.5 Fibril Length Distributions

Fibril length distributions for hIAPP were measured using atomic force microscope (AFM) by Peter Marek, State University of New York, Stony Brook, New York. The distribution used was from mature fibrils formed under conditions similar to the ones used in fibril kinetics assays in this thesis, supplementary material (53). These fibril length distributions for mature hIAPP reactions *in-vitro* were compared to model predictions of fibril length distributions at $t \to \infty$. Specifically, this data allows for an alternate means of determining

two key model parameters. One of these parameters is found in a way that relates directly to the kinetic Th-T data. The other relates to a specific stage of nucleation This is information that is not available from the Th-T data and gives validation to our theory.

4 Materials and Methods

To determine the kinetics of self assembly of hIAPP *in-vitro* a standard Th-T assay was used to produce kinetic profiles of fibril formation for various initial concentrations of the monomeric precursor protein. This data was systematically scaled and analyzed in the context of a generic nucleation-dependent polymerization model, based on mass action assumptions, which allows for secondary nucleation to occur through one of several pathways. Specifically, kinetic data for hIAPP fibril formation was collected from *in-vitro* experiments in Dr. Bruce Verchere's laboratory (Childrens' Hospital, Vancouver BC.). Fluorescence shift associated with the binding of Th-T to amyloid fibrils, but not beta sheet, monomer, or oligomeric species (56) was observed to capture monomer of hIAPP in fibril over time, for concentrations of monomers ranging from 10μM to 100μM.

4.1 Protein Preparation

Samples of 1mg hIAPP, were obtained in powdered monomeric form from (Bachem.com). The monomeric hIAPP was dissolved in 1000μL Hexafluoroisopropanol (HFIP) and aliquoted into 100μL units. The solubilized hIAPP was frozen at -20^oC for 2 hours, then moved to -80^oC overnight. Lyophilization was carried out the next day and the hIAPP was stored at room temperature until needed. Aliquots of hIAPP were dissolved in Dimethyl sulfoxide (DMSO) and mixed with filtered buffer, pH 7.4, in 500μL 96-well plates with 4μL Th-T, to the desired concentration of hIAPP. Buffer was prepared from filtered ($.2\mu$M) X10 stock diluted in distilled, filtered water. Rat IAPP, which does not form fibrils, along with "Blanks" (DMSO, Th-T, and buffer) were used as controls. Measurements were taken over a 20 hour period using a fluorescanner.

4.2 Fibril Elongation Kinetics

Fibril elongation kinetics were ascertained with a 50μM mature reactions which was vortexed for 30 sec. Monomeric hIAPP solutions of 25, 35 and 50 μM were added to the mature vortexed reactions and monitored with a Th-T assay. The first 600 seconds of the elongation kinetics were analyzed, assuming a constant number of fibril ends were present during this time.

4.3 Soluble Oligomer Filtration Assay

Filtration assays were conducted with centrifugal filter device from Millipore (ultrafree-MC Durapore PVDF 0.22um). It has been observed that hIAPP binds to this membrane,

thereby decreasing the level of hIAPP. In order to accommodate for this binding, membrane blocking with 10% skim milk in TBS was carried out. 100μL of this blocking solution was spun-down at 8,000rpm for 10mins. The membrane was then washed with distilled water. Washing was carried out by flushing the membrane surface with water. After washing the filter was spun-down for 4 minutes at 10,000rpm to rid the unit of residual water. The water was then removed by pipetting. This procedure prepared the filter unit for use with IhAPP. 10μL of the desired concentration of hIAPP was then mixed with 50μl of PBS just prior to filtration. This step compensates for the 10μL hold up volume associated with the units. The sample was centrifuged at 10,000rpm for 6 minutes, until all the solution had passed through the membrane. Blots of 2μL samples were placed on girded nitrocellulose membrane at 15 minute intervals for the first hour. Data points were then taken every 30 min for 2 hours then every hour, until 4 hours had passed. One final data point was collected at 24 hours. The membrane was allowed to air dry and was blocked with a 10% non-fat milk solution at 4^oC overnight. The membrane was then washed 3 times in a 1X TBST solution for 5 minutes. Primary antibody was then diluted in a 5% non-fat milk and 1X TBST solution. The membrane was then incubated under the solution for 1 hour with gentle shaking, and washed 3 times in 1X TBST for 5 min. Secondary antibody solution was made from diluted $.1\mu g/mL$ antibody in a 5% non-fat milk TBST solution. The membrane was then covered in this solution and incubated for 1 hour with gentle shaking. The membrane was then washed thee times in TBST solution for 5 min each washing. Substrate solution was then added and the images were developed and analyzed. The remainder of each sample was frozen at -80^oC at the time of sampling for later use.

4.4 Oligomer Time Course; Dot Blots

Oligomer time course assays were conducted using Dot Blots as described in the filtration section above, with two distinct differences. First, no filtration was used to separate non-soluble oligomers and fibrils from the solution prior to blotting the nitrocellulose membrane. Secondly, antibodies for oligomer staining as opposed to monomer antibodies were used. Furthermore, time points were taken at 15 and 30 minutes, at 1, 2, 3,6,8,10 hour time points. A final time point was taken at 24 hours. The Dot Blots were washed and incubated as above and developed within 24 hours.

5 Experimental Results

5.1 Kinetic Profiles for Fibrillogenesis

Kinetic profiles generated from Th-T assays, as described in Materials and Methods, resulted in characteristic sigmoidal curves as shown in Figure (1). Three distinct phases of the polymerization are noted from these kinetic profiles. 1) A pronounced lag phase of constant fluorescence where oligomers are formed but little monomer mass is in polymer form. 2) A rapid rise in fluorescence corresponding to an abrupt elongation of polymers that quickly accelerates. This elongation phase is notably shorter than the preceding lag phase over all concentrations. 3) A plateau in fluorescence that is approached exponentially, corresponding to a cessation of polymer formation. Furthermore, the maxima fluorescence A_∞ monotonically increases with increasing initial concentration of hIAPP. Conversely, the time required to reach the plateau in fluorescence monotonically decreases with increasing initial hIAPP concentration.

5.1.1 Scaled Data Collapse

Scaling of the experimentally observed fluorescence, $A(t)$, by its maximum value, A_∞, and t by a characteristic time, $t_0(A_\infty)$, resulted in approximate data collapse, as shown in Figure (2). Here we have arbitrarily used the time to 20% maximum fluorescence for $t_0(A_\infty)$. Plots of the log of A_∞ vs. the log of $t_0(A_\infty)$ result in a simple linear relationship. We see from Figure (3) that the slope of the best fit line of this plot is -2.09, auspiciously close to an integer. Thus, we note

$$\gamma \approx 2,$$

in the relationship

$$t_0(A_\infty) \propto A_\infty^{-\gamma},$$

and we may now impose this power law, a strict mathematical condition, on any model we use to describe the accumulation of monomers into fibrils. Furthermore, the collapse of all data sets over the given concentrations suggest the kinetics of hIAPP are largely independent of c_o, the initial monomer concentration. Therefore, all time-series data is approximately described by a single function,

$$A(t; A_\infty) = A_\infty f[t/t_0(A_\infty)],$$

resulting in the power law

$t_0 \propto A_\infty^{-\gamma}$,

for any model used to describe the data, where again γ is determined by the data as in Figure(3), see Appendix (11.1) for details.

5.2 Elongation Kinetics

Monomeric hIAPP solutions of 25, 35, 50 and 100μM were added to solutions of mature vortexed reactions made from 50μM initial monomer concentrations hIAPP and were monitored with Th-T assay, as described above in Materials and Methods. The first 600 seconds of fluorescence data show no lag phase and suggest fibril elongation begins swiftly. Furthermore, the rate of change in fluorescence is approximately constant over this period, Figure (4). These results are shown to be in agreement with fibril elongation by monomer addition.

5.3 Oligomer Time Course

Dot Blot data from oligomer time courses assays suggests oligomers form quickly in a concentration dependent manner and persist for at least 24 hours Figure (5). This time span is considerably longer than the time of formation for fibrils as fluorescence from the corresponding Th-T assays plateaus within 2 hours for the lowest concentration observed to produce fibrils. This observation is in agreement with similar assays that suggest oligomers of hIAPP persist on time scales longer than that of fibril formation.

5.4 Soluble Monomer and Small Oligomer Time Course

Unfortunately, all assays for soluble monomer conducted by the author, were unreadable and produced no discernable data. However, assays carried out by Miranker (6) using light scattering to detect soluble monomer concentration show soluble monomer concentration approaches 0 as fibril formation plateaus, Figure (6). These assay results are of particular importance as they support the key assumption in the model presented in this thesis, which states all monomers are "consumed" in the production of oligomers and fibrils. Furthermore, the mirroring of monomer depletion to that of fibril formation supports the assumption that most monomer mass is contained in monomers or fibrils. Likewise, this observation, especially at higher concentration, see Miranker and Evan (7,B), suggest that off-pathway kinetics which produce aggregate distinct from fibril formation play a minimal role, if any, in the kinetics of hIAPP fibrillation.

5.5 Cytotoxicity

Results from cell viability assays show an increase in cell toxicity as a function of initial monomer concentration, as well as time exposed to the fibril formation process, (data not

shown). This observation is in agreement with other assay results in the literature. Unfortunately, the assay is inconclusive as to the toxic component of hIAPP fibril formation. However, it suggests that the toxic affects are felt early in the process of fibril formation and continue to be present during fibril formation and after completion. This observation coupled with the observation that mature fibrils did not induce cytotoxicity in the absence of oligomers suggest that the toxic component in hIAPP fibrillogenesis is either the oligomers/aggregate populations or a result of maturing, (but not mature) fibrils. The last option seems unlikely.

6 Models of IAPP Polymerization

6.1 Simple Nucleation Dependent Polymerization

The Nucleation Dependent Polymerization model (NDP) is the basic model that describes the nucleated polymerization of a self assembling polymer. Monomers are assumed to quickly associate and dissociate, to form short-lived species, denoted oligomers. These oligomers are assumed to quickly come into steady state with the monomer population. Stable nuclei are then formed on a slower time scale and quickly elongate to form polymers. This model of a rate limiting nucleation process has been successful in describing actin(1,2) and microtubule (3,4) polymer formation. Furthermore, the kinetic profile generated by the NDP model is categorically sigmoidal. A brief review of a generic NDP model and the use of scaling, as presented by Flyvberg (3) for microtubule dynamics is given here in the context of IAPP fibrillogenesis. Following Flyvbjerg we let

$c(t)$ =IAPP monomer concentration,
$c(0) = c_o$ = the initial IAPP monomer concentration,
$c_i(t)$ =number concentration of the ith oligomer,
n_i =number of monomers added to c_i to form c_{i+1},
k =number of different oligomer species,
$\nu(t)$ = number concentration of nuclei,
$M(t)$ =monomer mass in fibril, excluding monomers in oligomer and nuclei,
f_i =forward rate constant for the ith oligomer species,
f_k =forward rate constant for nuclei formation,
f_{k+1} =forward rate constant for polymer elongation,
b_i =backward rate constant for the ith oligomer species,
d_i =disintegration rate constant for the ith oligomer species,
$A(t)$ = the measured fluorescence, assumed to be a measure of M.

Initially all mass is assumed to be in monomer form. These definitions, and the diagram shown in Figure(7), result in the following system of differential equations for nucleated polymerization. For the first oligomeric species we have

$$\frac{dc_1}{dt} = f_0 c^{n_0} - f_1 c^{n_1} c_1 + b_2 c_2 - d_1 c_1.$$

Here $f_0 c^{n_0}$ represents the rate of formation of c_1 as n_0 monomers bind together to form this species. This oligomeric species c_1 is also formed through the term $b_2 c_2$, representing the decay of the next oligomeric species c_2 into the c_1 species. The loss of c_1 oligomers to c_2 oligomers where n_1 monomers bind to c_1 forming c_2 is given by $-f_1 c^{n_1} c_1$. Finally, the c_1 oligomers may completely disassociated into monomers at a rate $d_1 c_1$. For the ith oligomer we have

$$\frac{dc_i}{dt} = f_{i-1}c^{n_{i-1}}c_{i-1} - f_i c^{n_i} c_i - b_i c_i + b_{i+1}c_{i+1} - d_i c_i, \quad \text{for } 2 \leq i \leq k.$$

The formation of the ith oligomer from the $i-1$ oligomer occurs by the addition of n_{i-1} monomers to the c_{i-1} species, represented by the term $f_{i-1}c^{n_{i-1}}c_{i-1}$. The ith oligomeric species is also created at a rate $b_{i+1}c_{i+1}$ through the loss of n_i monomers from the c_{i+1} oligomer species. Loss of the c_i species proceeds through the loss of n_{i-1} monomers from the ith species at the rate b_i, and is given by the term $b_i c_i$. Furthermore, c_i oligomers may be lost by the complete disintegration of the ith oligomer into monomers via the term $d_i c_i$. The equation for the change in concentration of stable nuclei is given by

$$\frac{d\nu}{dt} = f_k c^{n_k} c_k.$$

This equation represents the formation of stable nuclei ν by the binding of n_k monomers to the c_k oligomeric species, the largest oligomer allowed in the model.
Furthermore, the total change in mass of monomers in fibril form, discounting the monomer in oligomer and nuclei, is given by

$$\frac{dM}{dt} = f_{k+1} c\nu.$$

Conservation of mass, under our assumptions gives

$$-\frac{dc}{dt} = \frac{dM}{dt},$$

implying

$$c(0) = c(t) + M(t),$$

and

$$\frac{M(t)}{M_\infty} = 1 - \frac{c(t)}{c(0)} = \frac{A(t)}{A_\infty}.$$

Here, we have assumed that the mass of monomers in nuclei and oligomers is minimal compared to the mass in monomer or polymer form. This assumption is supported by soluble oligomer assays Figure (6) and Miranker (6).

6.1.1 Application of The Characteristic Scale to The Model

The generic model for nucleated polymerization presented above is now rescaled to eliminate the explicit dependence on c_o. Any model term left which explicitly contains c_o after the scaling must be set to zero, as described in (Experimental Results). We now enforce our scaling and the power law
$t_0 \propto A_\infty^{-\gamma}$,
on the system of differential equations requiring that c_o, the initial monomer concentration, not appear explicitly in the model. We use the following scaling variables

$$\hat{t} = \frac{t}{t_o}, \quad \text{and} \quad t_o \propto c_o^{-\gamma}.$$

Therefore,

$$\hat{t} = \frac{t}{\lambda c_o^{-\gamma}},$$

and

$$\hat{c} = \frac{c}{c_o}, \quad \text{with} \quad \hat{c}_i = \frac{c_i}{X}, \quad \text{for} \quad 2 \leq i \leq k,$$

where λ is needed to keep the units correct, and X is a quantity to be determined by the system. Likewise,

$$\hat{\nu} = \frac{\nu}{\mu}, \quad \text{and} \quad \hat{M} = \frac{M}{c_o},$$

where μ is a quantity to be determined by the system. Substituting the above into the model and requiring that c_o not appear explicitly in the equations reduces the model to

$$\frac{dc_1}{dt} = f_0 c^{2\gamma} - f_1 c^\gamma c_1,$$
$$\frac{dc_i}{dt} = f_{i-1} c^\gamma c_{i-1} - f_i c^\gamma c_i, \qquad \text{for } 2 \leq i \leq k,$$
$$\frac{d\nu}{dt} = f_k c^\gamma c_k,$$
$$\frac{dM}{dt} = f_{k+1} c \nu,$$

where the $\hat{}$ has been dropped, and λ has been absorbed into the reaction constants, Figure(8), Appendix (11.2).

The observation that the kinetic profiles of hIAPP fibril formation follow a systematic scaling and the implication that the initial monomer concentration is immaterial to the kinetics has allowed us to reduce the generic NDP model to one that uniquely describes the nucleated polymerization of hIAPP. However, we have no assurance that a single nucleation scheme, like the one presented above, is the correct description. We are, however, assured that of all the possible pathways allowed by the NDP model the one produced by our scaling is the only plausible candidate.

Fits of the scaled NDP model show a systematic error between the fits and the data Figures (9,10). Thus, the process of hIAPP fibril formation, as observed by Th-T assay, suggest that the NDP model is inadequate to describe the fibrillogenesis of hIAPP. Several alternate models have been suggested for the fibrillogenesis of hIAPP. Most are based on the NDP model and many additional off-pathways, which form oligomers through a process distinct from fibril formation. In this thesis we will examine some of the more prominent models in the literature. The power law discerned from the kinetic data will be used in each case to constrain the models. As we will see, the application of scaling and the power law to these proposed models will have a dramatic impact on their ability to describe the fibrillogenesis of hIAPP. Finally, we will present a simple dual nucleation model that allows both a primary nucleation, as described in the NDP model, with the added feature that fibrils promote a secondary nucleation event.

6.2 The Three-Stage Kinetic Model of Amyloid Fibrillation

A model similar to the NDP model by Lee et al. (33), has been put forth to describe the formation of amyloid fibrils in various disorders in a unified manner. However, through the "lens" of scaling and the use of elongation kinetics, we will see that the model reduces to the NDP model with a artificial scaling,

$$t_0 \propto A_\infty^{-\gamma}, \qquad \text{for } \gamma = 1.$$

Figure (11) shows a schematic of the proposed model for the species of interest. Here F denotes the fibril concentration and fibrils may elongate via addition of any oligomer to a fibril by the term

$$\sum_{j=1}^{k} l_j c_j F.$$

The concentration of fibrils F is similar to the number of nuclei formed in the NDP model above, and will be treated as such. Therefore, the assumption that negligible monomer mass is contained in oligomers and nuclei is extended to include the shortest of fibrils,

those containing a nuclei and 1 additional monomer. Given that the mean fibril length, in monomer units, is several orders of magnitude greater than the monomer units in a nuclei, this assumption seems plausible. The need to include these shortest fibers in the negligible mass pool assumption stems from the constraint that a fibril may only form by the addition of a monomer to a nuclei. Removal of this constraint should remove this new assumption. Here we precede with the convention used in (33). The rates of attachment and detachment for the ith oligomers to fibrils are given by l_i, and s_i respectively. Rewriting the model in the notation of this thesis, given the assumptions here and in Section [6.1] leads to the differential equations

$$\frac{dc}{dt} = -f_{k+1}cF + s_oF,$$

$$\frac{dc_1}{dt} = f_0c^2 - f_1c_1c + b_2c_2 - b_1c_1 + s_1F - l_1c_1F,$$

$$\frac{dc_i}{dt} = f_{i-1}c_{i-1}c - f_ic_ic + b_{i+1}c_{i+1} - b_ic_i + s_iF - l_ic_iF, \quad \text{for } 2 \leq i \leq k-1.$$

The change in the c_k species, and fibril tip populations are

$$\frac{dc_k}{dt} = f_{k-1}c_{k-1}c - f_kc_kc + b_{k+1}F - b_kc_k + s_kF - l_kc_kF,$$

and

$$\frac{dF}{dt} = f_kc_kc - b_{k+1}F.$$

Furthermore, we keep track of mass of monomers in fibril over time as well. The resulting equation for monomer mass in fibril is given by

$$\frac{dM}{dt} = f_{k+1}cF + \sum_{j=1}^{k} l_jc_jF - \sum_{j=0}^{k} s_jF - b_{k+1}F.$$

Systematic scaling of this model Appendix 11.3) results in the following system of equations

$$\frac{dc}{dt} = -f_{k+1}cF,$$

$$\frac{dc_1}{dt} = f_0c^2 - f_1cc_1 - l_1c_1F,$$

$$\frac{dc_i}{dt} = f_{i-1}cc_{i-1} - f_icc_i - l_ic_iF,$$

$$\frac{dc_k}{dt} = f_k c_{k-1} c - f_k c_k c - l_k c_k F,$$
$$\frac{dF}{dt} = f_k c_k c,$$

and

$$\frac{dM}{dt} = f_{k+1} c F + \sum_{j=1}^{k} l_j c_j F.$$

Elongation kinetics as described in section [7.2] suggest that fibril growth is mediated by monomer addition implying

$$l_i c_i F = 0, \quad \text{for } 1 \leq i \leq k.$$

Furthermore, the persistent population of oligomers observed experimentally cannot be established if the elongation terms for oligomeric species are not 0, or trivially small, Figures (12,13). The model now becomes

$$\frac{dc}{dt} = -f_{k+1} c F,$$
$$\frac{dc_1}{dt} = f_0 c^2 - f_1 c c_1,$$
$$\frac{dc_i}{dt} = f_{i-1} c c_{i-1} - f_i c c_i,$$
$$\frac{dc_k}{dt} = f_{k-1} c_{k-1} c - f_k c_k c,$$
$$\frac{dF}{dt} = f_k c_k c,$$

and

$$\frac{dM}{dt} = f_{k+1} c F = -\frac{dc}{dt}.$$

Therefore, the model as proposed in (33) results in a special case of the generic NDP model from the "view" of collapsible data and persistent oligomer populations, or elongation kinetics.

Removing the condition that only one monomer may join other monomers or oligomers to form the next oligomeric species, thus allowing the formation of each oligomeric species through any number of additional monomer units results in the NDP model

$$\frac{dc}{dt} = -f_{k+1}cF,$$

$$\frac{dc_1}{dt} = f_0c^{2\gamma} - f_1c^{\gamma}c_1,$$

$$\frac{dc_i}{dt} = f_{i-1}c^{\gamma}c_{i-1} - f_ic^{\gamma}c_i,$$

$$\frac{dc_k}{dt} = f_{k-1}c_{k-1}c^{\gamma} - f_kc_kc,$$

$$\frac{dF}{dt} = f_kc_kc^{\gamma},$$

and

$$\frac{dM}{dt} = f_{k+1}cF = -\frac{dc}{dt}.$$

Thus , we observe that the "Three-Stage Kinetic Model of Amyloid Fibrillation" reduces to the NDP model, under the systematic scaling and elongation kinetics implied by our data. Next we examine a NDP model that allows for off-pathway aggregates to form distinct from fibril formation.

6.3 Nucleation Dependent Model with Off-Pathway Kinetics for Aggregate Formation

We now look at a model for competing off-pathway aggregation by Powers and Powers (30). This type of model was proposed to account for the presences of oligomers found alongside growing and mature fibrils during amyloid fibrillogenesis. This model is similar to the model proposed by Chaung-Chung above, but has two distinct differences. Oligomers and fibrils are only allowed to grow through single monomer addition Again we see a problem only the scaling $\gamma = 1$ will satisfy this assumption in the model. The model imposes an off-pathway that allows oligomers to form in competition with the oligomers that lead to nucleated fibril formation. These off-pathway oligomers are referred to as aggregates. Powers and Powers noted in (30) that at some critical concentration of initial monomers scaling of data for fibril formation will become impossible. In the words of the authors

"We also find this mechanism has an especially striking feature: although increasing protein concentration generally cause simple nucleated polymerization to reach completion faster, they cause nucleated polymerization with off-pathway aggregation to reach completion more slowly when the protein concentration becomes too high."

We find this statement to be untrue for a specific subsystem of nucleated polymerization models with off-pathway aggregation. We will demonstrated bellow that this model does allow for the formation of persistent oligomers as both oligomers and aggregates. However, these aggregates are of the same size, in monomer units, as the oligomers that are formed during the nucleation process. Furthermore, the enforcement of the scaling law removes the back rate terms, see Appendix (11.1,11.2). We are left with a population of oligomers and aggregates that are monomericaly the same. Thus, no distinction can be made between the off-pathway aggregates and the on-pathway oligomers that are left after the monomer pool is consumed. Here we write the model proposed by Powers and Powers (30) in the notation of this thesis. The assumptions made for the basic NDP model apply here. However, Powers and Powers have imposed the arbitrary scaling

$$t_0 \propto A_\infty^{-\gamma}, \qquad \text{for } \gamma = 1.$$

The model allows nuclei to form through the addition of one monomer at a time to the preceding oligomeric species, for example, the c_i species is formed by the binding of a single monomer c to one of the c_{i-1} species at some rate f_{i-1}. The first oligomer being formed by two monomers binding to form c_1. Simultaneously, the model allows aggregate species z_1 to form by the binding of two monomers to form the first aggregate at some rate α_1. These aggregates may then grow by the addition of one monomer at a time to form the next aggregate species. Furthermore, aggregates and oligomers are allowed to lose monomers at any stage at some back rate β_i and b_i respectively. Using the notation in Section [6.1] and introduce the new variables and parameters

$z_i(t)$ =number concentration of the ith aggregate,
m =number of different aggregate species,
b_ν =backward rate constant for nuclei,
b_M =backward rate constant for fibrils,
α_i =forward rate constant for the ith aggregate species,
β_i =backward rate constant for the ith aggregate species,
Initially all mass is assumed to be in monomer form. These definitions, and the diagram shown in Figure(14) result in the following system of differential equations for nucleated polymerization of hIAPP with off-pathway aggregates. Here, as in section [6.1], we find the equations for the oligomeric species to be

$$\frac{dc_1}{dt} = f_0 c^2 - f_1 c c_1 + b_2 c_2 - b_1 c_1,$$

and

$$\frac{dc_i}{dt} = f_{i-1} c c_{i-1} - f_i c c_i - b_i c_i + b_{i+1} c_{i+1}, \quad \text{for } 2 \leq i \leq k.$$

Likewise, we see the formation of the aggregate species are

$$\frac{dz_1}{dt} = \alpha_0 c^2 - \alpha_1 z_1 c + \beta_2 z_2 - \beta_1 z_1.$$

$$\frac{dz_i}{dt} = \alpha_{i-1} z_{i-1} c - \alpha_i z_i c - \beta_i z_i + \beta_{i+1} z_{i+1}, \quad \text{for } 2 \leq i \leq m-1.$$

Furthermore, the change in the largest aggregate species if found to be

$$\frac{dz_m}{dt} = \alpha_{m-1} z_{m-1} c - \beta_m z_m.$$

We also obtain,

$$\frac{d\nu}{dt} = f_k c^{n_k} c_k - b_\nu \nu.$$

This equation represents the formation of the unstable nuclei ν by the binding of n_k monomers to the c_k oligomeric species, the largest oligomer allowed in the model, and allowing decay through the term $-b_\nu \nu$. Furthermore, the total mass of monomers in fibril form, discounting the monomer mass in oligomer, aggregate and nuclei is given by,

$$\frac{dM}{dt} = f_{k+1} c \nu - b_M \nu.$$

The term $-b_M \nu$ allows for the loss of monomers from the total mass of monomers in fibrils, which is proportional to the number of fibril ends present. Here we have assumed that the number of fibril ends present is equal to the number of nuclei formed. Since nuclei form slowly and elongation is rapid this assumption is a reasonable one, as no breaking of fibrils is allowed in the model. We now introduce the additional scaled variable

$$\hat{z}_i = \frac{z_i}{Y}, \qquad \text{for } 1 \leq i \leq m,$$

here Y is to be determined by the system. Substituting the scaling variables into the model and dropping the $\hat{}$s gives

$$\frac{dc_1}{dt} = \lambda[f_0 c^2 - f_1 c_1 c],$$

$$\frac{dc_i}{dt} = \lambda[f_{i-1} c_{i-1} c - f_i c_i c c], \quad \text{for } 2 \leq i \leq k,$$

$$\frac{d\nu}{dt} = \lambda[f_k c_k c],$$

and

$$\frac{dM}{dt} = \lambda[f_{k+1}\nu c].$$

Furthermore, the rates of change for the off-pathway aggregates become

$$\frac{dz_1}{dt} = \lambda[\alpha_0 c^2 - \alpha_1 z_1 c],$$
$$\frac{dz_i}{dt} = \lambda[\alpha_{i-1} z_{i-1} c - \alpha_i z_i c], \quad \text{for } 2 \leq i \leq m-1.$$

The change in the largest aggregate, in monomer units, is now given by

$$\frac{dz_m}{dt} = \lambda[\alpha_{m-1} z_{m-1} c].$$

Therefore, we find, given our data constraints, that the "Nucleation Dependent Model with Off-Pathway Kinetics for Aggregate Formation" reduces to the NDP model where aggregates of the same monomeric size as oligomers are produced. Furthermore, these aggregate populations are ever increasing, and given that no "bottleneck" of nucleation exist along the aggregate pathway it is likely that such aggregation events would effectively compete for monomers, especially during early stages of fibrillogenesis. The result is a notable mass of monomers being sequestered into aggregates. This would contradict our assumption that all appreciable monomer mass is in either fibril or monomer during the fibril formation process, a prediction not supported by experimental data Figure (6). This model may be easily modified in such a way that allows for any scaling of γ, Figure (15). However, the observation that the off-pathway aggregates will be of the same size in monomer units as the persistent oligomer population will hold, except perhaps for the smallest aggregate species, see Appendix (11.2).

6.4 A Generic Nucleation Dependent Model with Off-Pathway Kinetics for Aggregate Formation

We now rewrite the nucleation dependant model with off-pathway aggregates where oligomers and aggregates are allowed to form by any number of monomers joining to form the first species. Subsequent species are allowed to form by binding to any number of monomers to form the next largest species. No constraint is imposed that requires oligomers and aggregates to be made of the same number of monomer units. However, aggregates may only form from monomers and other aggregates, likewise oligomers may only form from monomers and other oligomers. We now introduce the additional parameter

a_i =number of monomers added to z_i to form z_{i+1}.

Then the diagram shown in Figure(15) and our standard assumptions result in the following system of differential equations for nucleated polymerization with off-pathway aggregates. The differential equation for the oligomeric and aggregate species are now given by

$$\frac{dc_1}{dt} = f_0 c^{n_o} - f_1 c_1 c^{n_1} + b_2 c_2 - b_1 c_1,$$

$$\frac{dc_i}{dt} = f_{i-1} c_{i-1} c^{n_{i-1}} - f_i c_i c^{n_i} - b_i c_i + b_{i+1} c_{i+1}, \quad \text{for } 2 \leq i \leq k,$$

and

$$\frac{dz_1}{dt} = \alpha_0 c^{a_o} - \alpha_1 z_1 c^{a_1} + \beta_2 z_2 - \beta_1 z_1.$$

$$\frac{dz_i}{dt} = \alpha_{i-1} z_{i-1} c^{a_{i-1}} - \alpha_i z_i c^{a_i} - \beta_i z_i + \beta_{i+1} z_{i+1}, \quad \text{for } 2 \leq i \leq m-1.$$

The change in the largest aggregate species allowed is

$$\frac{dz_m}{dt} = \alpha_{m-1} z_{m-1} c^{a_{m-1}} - \beta_m z_m.$$

We also obtain

$$\frac{d\nu}{dt} = f_k c^{n_k} c_k - b_\nu \nu.$$

Furthermore, the total mass of monomers in fibril form, discounting the monomer in oligomer, aggregate and nuclei, is given by

$$\frac{dM}{dt} = f_{k+1} c\nu - b_M \nu.$$

Substituting our scaling variables into the model and dropping the $\hat{}$s gives, see Appendix(11.2)

$$\frac{dc_1}{dt} = \lambda[f_0 c^{2\gamma} - f_1 c_1 c^{\gamma}],$$

$$\frac{dc_i}{dt} = \lambda[f_{i-1} c_{i-1} c^{\gamma} - f_i c_i c^{\gamma}], \quad \text{for } 2 \leq i \leq k,$$

$$\frac{d\nu}{dt} = \lambda[f_k c_k c^{\gamma}],$$

and

$$\frac{dM}{dt} = \lambda[f_{k+1}\nu c].$$

Furthermore, the rates of change for the off-pathway aggregates become

$$\frac{dz_1}{dt} = \lambda[\alpha_0 c^{a_o} - \alpha_1 z_1 c^{\gamma}],$$
$$\frac{dz_i}{dt} = \lambda[\alpha_{i-1} z_{i-1} c^{\gamma} - \alpha_i z_i c^{\gamma}], \quad \text{for } 2 \leq i \leq m-1.$$

The change in the largest aggregate, in monomer units, is now given by

$$\frac{dz_m}{dt} = \lambda[\alpha_{m-1} z_{m-1} c^{\gamma}].$$

Thus, we see that given fibril formation data that scales systematically, as is in the case in hIAPP fibrillogenesis, off-pathway kinetics are restricted, mathematically, in the same way as are the on-pathway kinetics of nuclei formation and no distinction can be made between such events Figure (16). Furthermore, the time scale of formation of aggregates is likely faster than the fibril formation time scale due to the "Bottleneck" step at the nucleus. Therefore, aggregate populations can either be assumed to be in equilibrium with the monomer population on the time scale of fibril formation, implying fibril formation will not scale for high initial monomer concentrations, or the back-rate terms in the aggregate kinetics must be trivially small, while aggregate sizes in monomer units is restricted to mirror oligomer sizes. We therefore state that off-pathway kinetics for aggregate formation is unlikely a pronounced feature of hIAPP fibril formation and is redundant in this class of models, given the constraints provided by our data. The presence of such terms will only go to alter formation rates in data fits, and give no new insight into the structure of these aggregates. Therefore, models with off-pathway aggregates may fit the kinetics profiles of fibril formation that scale under all initial monomer concentrations, which result in fibril formation. However, they introduce an unneeded pathway, from a mathematical point of view. We also note that, under scaling, populations of aggregates will increase until the monomer population is depleted. This competition of aggregates vs. fibrils for monomers could have a notable impact on the total oligomer/aggregate populations, if aggregate formation rates are not trivially small, resulting in the production of a notable oligomer/aggregate population. However, plots of the sum of normalized monomer and fibril mass populations suggest that oligomer and aggregate populations are trivially small for all times, Figure (6). Furthermore, this model, like all single nucleation models, does not readily fit the kinetic profile observed for hIAPP and exhibits a systematic error in

these fits, Figures (9,10). Given these observations, we propose a model for the nucleated polymerization of *h*IAPP that does not have an off-pathway for aggregate formation, but does consist of a secondary fibril-mediated nucleation step. This step is left generic, surface mediated nucleation, branching or breaking are all allowed as ways to form new nuclei (fibril ends) on which elongation may occur. The scaling law observed from the data collapse and the corresponding power law are then employed to reduce the rather generic model to the unique model, under our assumptions, that describes the data.

7 Generic Nucleation Model with Fibril-Dependent Secondary Nucleation

Using the NDP model, as described above, we now allow nuclei to form through a secondary fibril-dependent process Figure(17). After application of the scaling law the model reduces to Figure (18)

$$\frac{dc_1}{dt} = f_0 c^{2\gamma} - f_1 c^{\gamma} c_1,$$

$$\frac{dc_i}{dt} = f_{i-1} c^{\gamma} c_{i-1} - f_i c^{\gamma} c_i, \quad 2 \leq i \leq k.$$

However, for some species class j we have

$$\frac{dc_1}{dt} = f_0 c^{2\gamma} - f_1 c^{\gamma} c_1 - \delta f_j c^{(\gamma-1)} c_j M, \qquad \text{if } j = 1,$$

or

$$\frac{dc_j}{dt} = f_{j-1} c^{\gamma} c_{j-1} - f_j c^{\gamma} c_j - \delta f_j c^{(\gamma-1)} c_j M, \qquad \text{for some } 2 \leq i = j \leq k,$$

and

$$\frac{d\nu}{dt} = f_k c^{\gamma} c_k + \delta f_j c^{(\gamma-1)} c_j M,$$

$$\frac{dM}{dt} = f_{k+1} c \nu.$$

Here δ may be interpreted as either a scaled branching, breaking or catalyzing rate. These phenomena are largely indistinguishable in the current model analysis, however data fits clearly separate these possibilities. Fits of the model to the data give consistent estimates for all parameters, and convincing fits to the data Figures(19,20). An interesting prediction of this class of scaled models is that as the last monomers are sequestered into polymers they leave behind oligomeric species. Neither the off-rates, b_i, nor the disintegration rates, d_i, are relevant to the kinetics, within the detection level of our assay, and no observable net flux of monomers into or out of the various oligomer species exist due to these terms. Typical residual oligomer populations and their rates of formation are shown in Figures(21,22) respectively.

7.1 Equation Number and Initial Formation Kinetics

In order to determine the equation number, the number of steps required to form a nuclei, we have several options. One could simply fit the scaled model with k as a fitting parame-

ter. Likewise, one may use k as a slowly varying parameter in data fits of the scaled model. A third option involves extrapolating the slope of the kinetic profile for early times on a *log log* scale, giving the order of initial fibril formation and thus k. Here we have chosen to evaluate the model at early times giving a first order solution for the scaled model in t. This first order solution is then fit to the data for early times, just as the initial rise in Th-T fluorescence is observed and before fibril kinetics accelerate, implying secondary effects have become impactful. As a check of our first order solution for the number of nucleation equations k we then plot both the observed time to 50% completion t_{50} versus the predicted time to 50% completion t_{p50} on a *log log* plot, Figure (23). Here, as with t_0 our scaling time, t_{50} is an arbitrary choice and the analysis follows through with any chosen time of completion. We now determine the initial formation kinetics of hIAPP by approximating the model as a first order system close to $t = 0$, with

$$\frac{dc_1}{dt} = f_0 c^{2\gamma},$$
$$\frac{dc_i}{dt} = f_{i-1} c^{\gamma} c_{i-1},$$
$$\frac{d\nu}{dt} = f_k c^{\gamma} c_k,$$
$$\frac{dM}{dt} = f_{k+1} c\nu.$$

Solving the equations successively leads to

$$c_1 = f_0 c_o^{2\gamma} t,$$

$$c_i = \prod_{j=0}^{i-1} f_j \frac{c_o^{(i+1)\gamma}}{i!} t^i, \qquad \text{for } 2 \leq i \leq k.$$

We then obtain

$$\nu = \prod_{j=0}^{k} f_j \frac{c_o^{(k+2)\gamma}}{(k+1)!} t^{k+1},$$

and

$$M = \prod_{j=0}^{k+1} f_j \frac{c_o^{(k+2)\gamma+1}}{(k+2)!} t^{k+2}.$$

k was determined by fitting $A = \alpha_1 t^{k+2} + \alpha_2 t^{k+3}$ to the fluorescence data for hIAPP, such that $\alpha_1 \gg \alpha_2$, to assure we have the first order solution to the model. We thus obtain the nucleation size $N = (k+2)\gamma$, where, again, γ is determined by the fit of the log of $t_0(A_\infty)$ vs. the log of (A_∞), as described in [5.1]. It may be read off as the slope of the

best fit line in Figure(3), Appendix (11.1). Plots of the observed time to 50% completion vs. theoretical time to 50% completion are shown in Figure (23). We see excellent agreement between the theoretical and observed formation rates of fibrils, and the parameter, k, with the theoretical value of k as determined by first order solution of the scaled model.

7.2 Elongation Kinetics

Monomeric hIAPP solutions of 25, 35, 50 and 100μM were added to mature vortexed reactions made from a 50μM solution and monitored with Th-T assay as described above in Materials and Methods. The first 600 seconds of fluorescence data show no lag and suggest fibril elongation begins swiftly. Furthermore, the rate of change in fluorescence is approximately constant over this period Figure (4). Assuming elongation occurs by addition of oligomers of monomer size n_f to fibril ends F at the rate f_e, and that all appreciable monomer mass is in either monomer or polymer form. We have

$$-\frac{dc}{dt} = f_e F c^{n_f},$$

and

$$\frac{dM}{dt} = -\frac{dc}{dt}.$$

Given the assumption that the fluorescence $A(t)$ is a measure of the mass of monomer in fibril $M(t)$, we may write

$$\frac{dA}{dt} = f_e F c^{n_f}.$$

A plot of

$$\log \frac{dA}{dt} \text{ vs. } \log(c_o),$$

gives a slope of $n_f = 1$ as shown in Figure(24). Thus we find, elongation of hIAPP fibrils is well described by monomer addition. The same elongation kinetics were found monitoring monomer consumption directly by Miranker for seed concentrations ranging from 1ηM to 100μM added to 50μM vortexed reactions (6).

7.3 Fibril Length Distribution

The Th-T assay gives no direct information about the number or length of fibrils. Nonetheless, we are able to develop a relative length distribution for fibrils for any time $t = \bar{t}$

$$p(l; \bar{t}).$$

Given our lack of data about fibril length or number of fibrils, we look for a "scaled" distribution, that is, we normalize our length distribution to 1. Mathematically we write

$$\int_0^\infty p(l;\infty)\,dl = 1.$$

Furthermore, the fibril length our distribution depends on is a relative one and is normalized to 1

$$\int_0^\infty p(l;\infty) l\,dl = 1.$$

Given the rate of formation of fibrils at any time t

$$\frac{d\nu}{dt} = f_k c^\gamma c_k + \delta f_j c^{(\gamma-1)} c_j M,$$

and the corresponding "velocity" of fibril growth

$$f_{k+1} c(t).$$

We can determine the length l, at time $t = \infty$, of a given fibril that formed at time t

$$l = f_{k+1} \int_t^\infty c(t')\,dt'.$$

Using the rate of formation of fibrils, the fibrils of length l to $l+dl$ at time $t = \infty$ is simply

$$p(l;\infty)dl = \frac{d\nu}{dt}dt.$$

Therefore, we have

$$p(l;\infty) = \frac{f_k c^\gamma c_k + \delta f_j c^{(\gamma-1)} c_j M}{f_{k+1} c(t)}.$$

This distribution is shown over data points collected by Peter Marek in figure (25). The plot of the length distribution at large time was generated by fitting the scaled nucleation model with fibril-dependent secondary nucleation to scaled data for an arbitrary initial monomer concentration. No attempt was made to directly fit the model length distribution to the experimental length distribution data. To view the distribution for early times one simply shifts the horizontal axis to the left.

7.4 Impact of Parameter Variation on Fibril and Oligomer Populations

Variations in the rates of formation of fibrils and nuclei result in predictable changes in populations of total oligomers, number of fibrils formed, and, obviously, the time scale of fibril formation. These observations are summarized in Figures (26, 27). These plots suggest that blindly slowing or inhibiting fibril elongation rates is not the most prudent course for reducing cytotoxicity of hIAPP fibrillogenesis, given that total oligomer and fibril densities both monotonically increase as elongation kinetics are retarded. Thus, slowing of fibril elongation, without completely preventing it, will result in greater numbers of short fibrils and an increased number of oligomers. Retarding nuclei formation rates has a similar effect on oligomer populations. However, fibril densities are impacted in the reverse manner. Therefore, lowering fibril nuclei formation rates will result in an increased oligomer population, but will have the effect of reducing total fibril density, revealing a potential avenue of research for determining the cytotoxic component in hIAPP fibrillogenesis. Given these observations, this model may prove useful in screening potential therapeutic drugs for type II diabetes treatment. Specifically, kinetic profiles in the presence of inhibiters may be analyzed in the context of this model to detail the exact mechanism by which the inhibitor affects the fibril formation process. Furthermore, the resulting impact on oligomer population, the relative number of fibrils produced and the length distributions may be determined readily using the model, given nothing more than the kinetic profile of fibril formation, as measured by relative mass of monomers in fibril form. We note that, the observation of accelerated fibril kinetics reducing both fibril density and oligomer populations is in qualitative agreement with assays suggestion accelerated fibril formation decreases cytotoxicity.

7.4.1 Impact of Heparin on The Formation Kinetics of hIAPP

Heparin, a widely used anticoagulant with a known molecular structure, has been assessed for its ability to impact fibril formation using a Th-T assay as described above in (Materials and Methods). We find the presence of heparin rapidly accelerated the formation of amyloid fibrils *in-vitro* Figure (27). Fits of the scaled nucleation model with fibril-dependent secondary nucleation suggest that both primary and secondary nucleation are drastically accelerated. However, examination of the fluorescence profiles of several initial concentrations of hIAPP monomer with constant heparin concentration does not produce scalable data. Therefore, the theory presented here and its results do not apply to the observed fibrillogenesis of hIAPP in the presence of heparin. Furthermore, the lack of scaling specifically preclude the subclass of models isolated here for hIAPP fibril formation. Thus, we may conclude that heparin results in the inclusion of non-scalable terms in any NDP model which describes it and implies that heparin acts to increase the trivially small reverse rates of oligomer and/or fibril decay that we have removed from our model of hIAPP fibrillogenesis on phenomenological bases. This supposition is further

supported by the observed decrease in fluorescence seen in the profiles in Figure (28) just after maximum fluorescence is reached.

7.5 Relevance to Current Biological Hypotheses

Many current biological arguments suggest that hIAPP precursor protein may undergo a separate aggregate pathway that is distinct from fibril formation. This alternate pathway has been invoked to account for potentially toxic oligomeric species that are seen alongside growing, and mature fibrils. Experimental evidence about the exact life-times of these oligomeric species is unclear. However, onset of oligomer formation is rapid and begins well before the first fibrils are observed. Furthermore, experimental evidence suggests a life-time of the oligomeric species of an order of magnitude or greater than the growth kinetics of fibrillogenesis in IAPP, Figure(5). The above model gives a natural candidate for these oligomeric species, without the need for a separate off-pathway for aggregate formation, namely the oligomers that are "trapped" after the depletion of the monomer pool, unable to grow or decay. It should be noted that we have determined that neither the off-rates, b_i, nor the disintegration rates, d_i, are relevant to the kinetics and that no net flux of monomers into or out of the various oligomeric species exist due to these terms, within the detection level of the Th-T assay. A small net flux of monomers may exist that is too small to be detected by our assay. Simulations suggest that such a small net flux of monomers would have a minimal impact on the results presented here, and would allow for the decay of oligomers as some experiments imply.

8 Conclusions

The observation that various initial concentrations of hIAPP monomer result in fibril formation kinetics *in-vitro*, as observed with Th-T assays, that systematically scale and collapse onto a single profile, gives considerable insight into the kinetics of fibril nucleation and elongation. Specifically, the scaling relationship puts strict constraints on any nucleation model used to describe hIAPP fibrillogenesis. These constraints, as detailed above, allow for the systematic removal of superfluous terms in the model which are not justified by the formation kinetics under scaling, but would be considered prudent to include, in general, in the modeling of nucleated polymer kinetics. For example, the back rates of oligomer formation are often included in such models and are needed, in many cases, to describe the polymerization event in question. However, inclusion of these terms in a model that describes scalable data is not only unsupported, but may lead to misleading results for model fits. Blind fitting of models to data for hIAPP with out the removal of non-scalable terms, as implied by data collapse, has led to suggestions that off-pathway kinetics play a role. While the use of scaling to reduce fibril formation models does not preclude the existence of off-pathway kinetics, it does put rather harsh restrictions on the allowed kinetics of the off-pathway aggregates. Specifically, any off-pathway aggregate is constrained to the same scaling as on-pathway oligomers, (except for perhaps the smallest aggregate), and will have the same size in monomer units, be formed and grow by the same number of monomer units at each step in assembly, and are mathematically and kinetically indistinguishable.

Given these observations the simplest model that accurately fits the kinetic profile for hIAPP fibril formation, and does not violate the observed scaling of these profiles, is a nucleation dependent polymerization model with fibril-dependent secondary nucleation and no off-pathway aggregates, as described in section [7]. Thus, phenomenological modeling of fluorescence shift associated with Th-T binding to hIAPP fibrils suggests that *fibril formation is dominated by a primary nucleation event and facilitated by a rapid secondary nucleation event that is fibril dependent.* Scaling arguments and first order solutions for early times to the described model indicate that nuclei are formed in five steps. First, four monomers combine to form the first sub-nuclei c_1, then two monomers bind to c_1 forming c_2. This addition of monomer pairs continues until c_4, after which a stable nucleus of twelve monomers is formed from c_4 by addition of two monomers. Fibrils then grow by unit addition. As fibrils form, a secondary fibril-dependent nucleation occurs by addition of a single monomer to the c_4 species. These secondary nuclei then form fibrils by unit addition. The results are summarized in Figure (18).
To quote Flyvberg

"Thus, by combining a simple, but precise, physical measure with a systematic mathematical analysis we have created a "microscope" through which one apparently may

"observe" some otherwise inaccessible details of a biochemical self-assembly process."

Through the "lens" of this "microscope" we can observe the kinetics of assembly of oligomers, nuclei and fibrils on an arbitrarily fine scale, thus allowing for the determination of an exact process of assembly. One should keep in mind that this process, while mathematically rigorous, is not guaranteed to be correct. For example the NDP model scales in accordance with the data, but does not accurately describe the formation of hIAPP fibrils as observed by Th-T assay. We have simply found a detailed model for hIAPP fibril formation which describes all observed data and does not violate the condition that various initial concentrations of hIAPP monomer produce kinetic profiles that will collapse to one "master" profile, when subjected to a systematic mathematically rigorous scaling. While this scaling is not perfect, it is accurate to a high degree, so that it is difficult to discern if the small violations in data collapse are due to a systematic error or experimental error associated with the assays. Nevertheless we can investigate a systematic error in the scaling violation observed by looking at late times in fibril formation, section [8.2].

8.1 Self Consistency of The Assumption of Trivial Monomer Mass in Oligomer Populations

A crucial assumption in our model is that the mass of monomers in oligomers and nuclei is trivially small compared to the mass in fibrils and monomers for all times. This assumption has allowed us to relate the experimentally determined value of fluorescence $A(t)$ to the initial monomer concentration $c(0)$. The latter is difficult to determine with a high degree of accuracy, while preserving the accuracy with which we measure the fluorescence. We have shown this assumption to be approximately true experimentally, Figure (6). However, we may also look for the self consistency of this assumption by using the theoretical values of the oligomer populations, as determined by our model, using the equation

$$c(t) + M(t) = c(0).$$

Inserting the model predictions for oligomer and nuclei population values into the exact equation for monomer mass

$$c + n_o c_1 + (n_0 + n_1)c_2 + ... + \sum_{i=0}^{k-1} n_i c_k + \sum_{i=0}^{k} n_i \nu + M = c(0).$$

We now observe that these additional terms are trivially small for all time. Thus, we are able to work in the scaled variable $c(t)/c(0)$ and we are justified in assuming that

$$M(t)/M_\infty = 1 - c(t)/c(0).$$

Therefore, we preserve the precision with which we measure fluorescence without introducing any uncertainty from the biochemical assay of c(0) into our model.

8.2 Room for Improvement

The theory presented above is only approximate. Specifically, if the theory were exact, the observed scaling would be exact and not deviate as observed in Figure (2). We may observe this by noting that if the relationship

$$t_0(A_\infty) \propto A_\infty^{-\gamma},$$

were exact then the characteristic time t_∞ defined as

$$A_\infty - A(t) \propto \exp(-t/t_\infty),$$

would be constant for all A_∞. However, Figure (29) shows that t_∞/t_o is only approximately constant, there is some dependance on A_∞. Furthermore, we may note, from Figure (1), that fluorescence and therefore mass in fibril, M, does not monotonically increase for all times but exhibits a slight drop after reaching maximum fluorescence, a feature our system of differential equations cannot describe. It is worth noting however, that this violation of t_∞/t_o independent of A_∞ is observed by looking at later times and does not imply a grave contradiction to the modeling procedure presented here.

8.3 Qualitative Failure of Ordinary Differential Equations to Explain All Observed Phenomenon

Again, looking at late times in fibril formation reveals a qualitative feature which is beyond the scope of a finite system of ordinary differential equations to describe. Specifically, plots of t/t_o vs. $1 - A(t)/A_\infty$, at lower concentrations, suggest that the slope of the time series decreases slightly at later times, thus implying that fibrils are lost. This is in contradiction to the assumption that fibrils only grow and is a violation of the prediction of our model, which says the slope of these plots are described by

$$\frac{d}{dt} log_{10}(A_\infty - A(t)) = \frac{d}{dt} log_{10} c(t) = \frac{-c_o}{M_\infty} f_{k+1} \nu(t).$$

Here we have used the fact that

$$\frac{M(t)}{M_\infty} = 1 - \frac{c(t)}{c(0)} = \frac{A(t)}{A_\infty},$$

and

$$\frac{dM}{dt} = f_{k+1} c \nu.$$

We observe that fibrils cannot disappear,

$$\frac{d\nu}{dt} = f_k c^\gamma c_k.$$

This observation has allowed us to write the equations for mass in fibril in a finite set of equations. Therefore, no theory based on a finite number of differential equations can describe the observed phenomenon exactly and a model tracking both growing and shrinking fibrils and their distributions is needed. This observation implies that a more exacting model of the fibrillogenesis of hIAPP would require partial differential equations. Therefore, we state that the theory presented here is accurate for the maximum number of fibrils formed which is approximately equal to the number of fibrils at t_∞, and our model is most accurate up until this time t_{max}, where this time to maximum fibril density is defined as

$$t_{max}^{-1} = max[-\frac{d}{dt} log_{10}(A_\infty - A(t))].$$

Therefore, we note that, despite the seemingly limited amount of information in our simple assay, we have yet to exhaust all the information about the formation of fibrils that is contained in the data.

9 Figures

9.1 Experimental Fluorescence Data

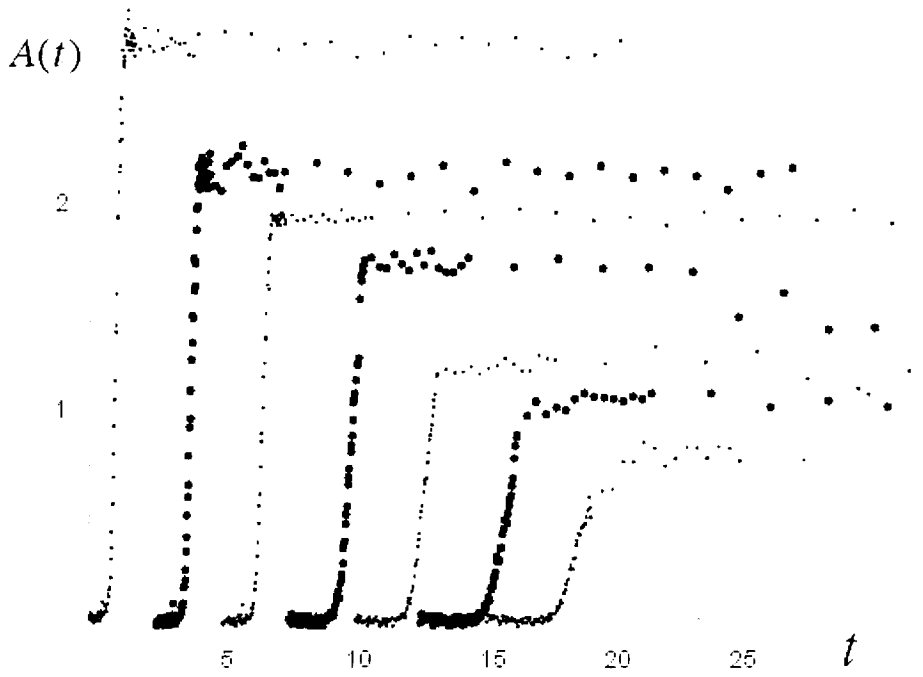

Figure 1: Characteristic sample of the fluorescence of Th-T, $A(t)$ (vertical axis), for initial monomer concentrations of hIAPP from 25 to 100 μM, right to left respectively. Each data set has been scaled in fluorescence and shifted along the t axis's (horizontal axis) incrementally by $\delta t = 2.5$, for ease of viewing individual plots. This data shows three distinct phases of fibril formation. 1) A pronounced lag phase of constant fluorescence where nuclei are formed. 2) A rapid rise in fluorescence corresponding to an abrupt elongation of polymers. 3) A plateau in fluorescence that is approached exponentially, corresponding to an exponential decrease in polymer formation. Furthermore, the maximum fluorescence, A_∞, monotonically increases with increasing initial concentration of hIAPP. Conversely, the time required to reach the plateau in fluorescence monotonically decreases with increasing initial hIAPP concentration.

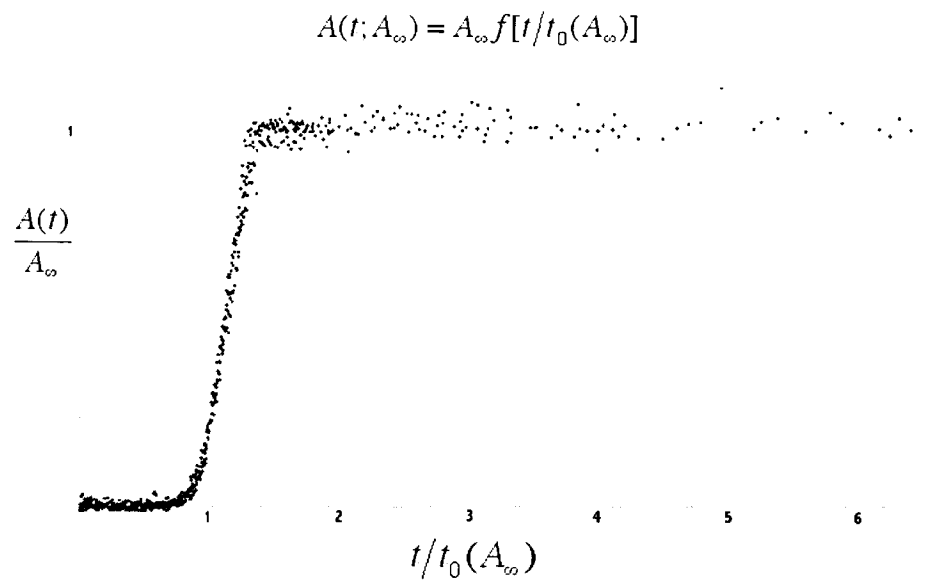

Figure 2: Scaled fluorescence data of Th-T, $A(t)/A_\infty$ (vertical axis) versus scaled time $t/t_0(A_\infty)$ (horizontal axis) . Each data set has been divided by its maximum recorded florescence, A_∞, for various initial monomer concentrations of hIAPP from 25 to 100μM. Likewise, each data set has been scaled by $t_0(A_\infty)$, the time recorded for that data set to reach 20% maximum fluorescence, A_∞. This approximate collapse of data for all assayed initial concentrations of hIAPP allows us to form a model for the mass of monomers in polymer form that is independent of the initial concentration of monomers. Furthermore, this data collapse, given certain assumptions, allows us to work with scaled variables. We have effectively removed any uncertainty in initial monomer concentrations from our data and subsequent model calibrations and fits.

9.2 Power Law

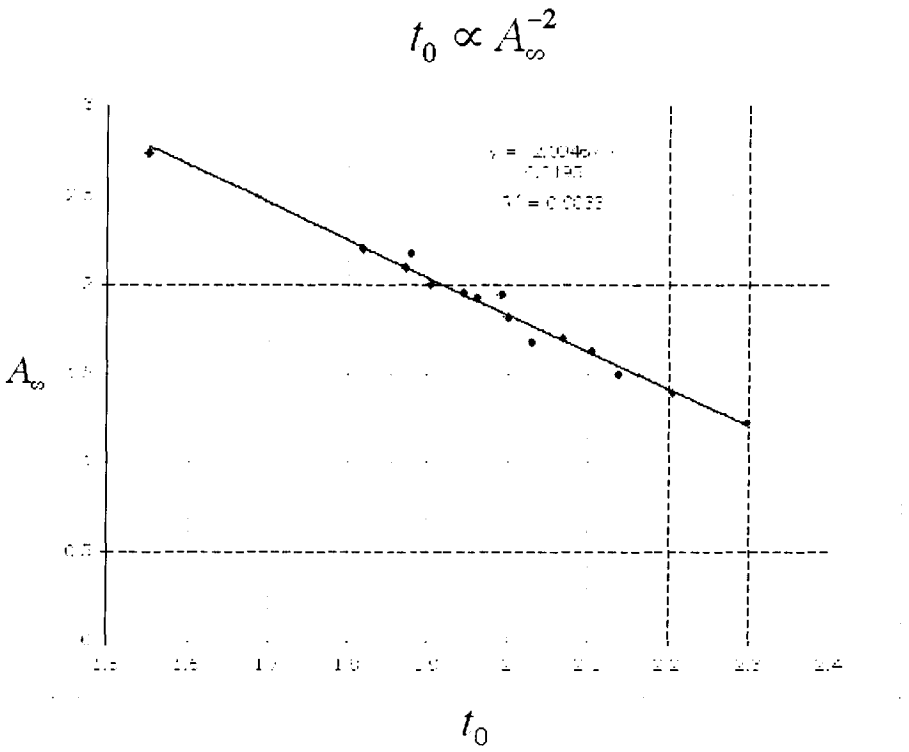

Figure 3: Log(A_∞) (vertical axis) plotted against Log($t_0(A_\infty)$) (horizontal axis) for several data series between 20 and 100μM of initial hIAPP monomer. Here we see the slope of the best fit line is -2.09, auspiciously close to an integer. Thus, we note $\gamma \approx 2$ in the relationship $t_o(A_\infty) \propto A_\infty^{-\gamma}$ and we may now impose this power law, a strict mathematical condition, on any model we use to describe the accumulation of monomers into fibrils

9.3 Fluorescence of Seeded Reactions

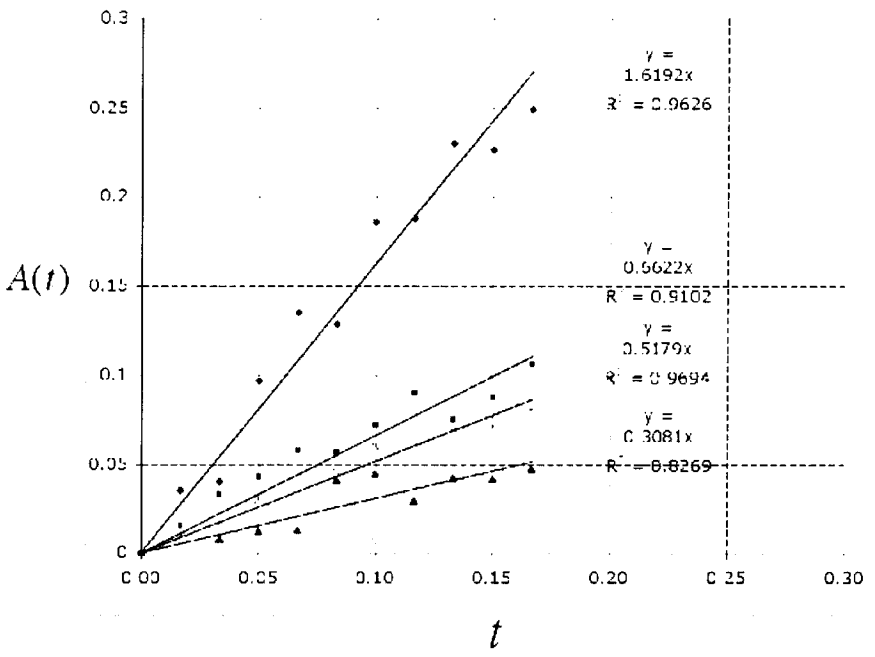

Figure 4: Fluorescence for seeded reactions of hIAPP (vertical axis) versus time (horizontal axis). Initial concentrations of 25, 35, 50 and 100μM monomers were added to "seeds" generated from vortexed 50μM initial monomer concentration mature reactions of hIAPP. The rate of changes in fluorescence, corresponding to the slopes of the best-fit lines, are used in determining the kinetics of elongation.

9.4 Experimental Oligomer Concentrations

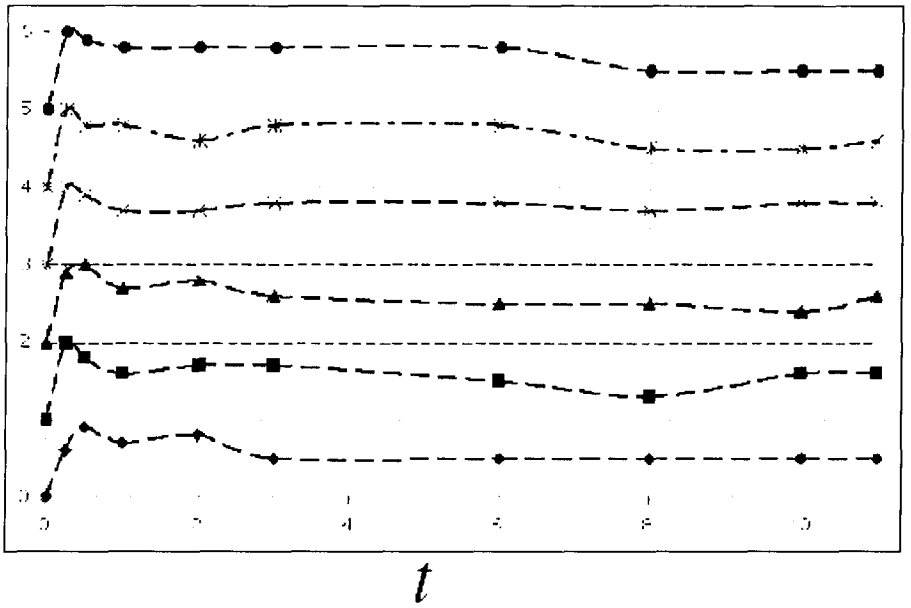

Figure 5: Relative oligomer abundance for initial monomer concentrations of 25, 30, 35, 40, 45, and 50μM hIAPP, from bottom to top respectively. Each data set is plotted on a normalized y axis, 0 to 1, with each data set being shifted vertically 1 unit for visibility. The data suggest that oligomers form quickly and are found at their maximum concentrations within the first 15 minutes in most cases and by 30 min in all cases. Furthermore, all concentrations exhibit a persistent oligomer population for at least 24 hours of approximately 50-60% of the maximal oligomer concentration.

9.5 Monomer and Monomer in Fibril Comparison

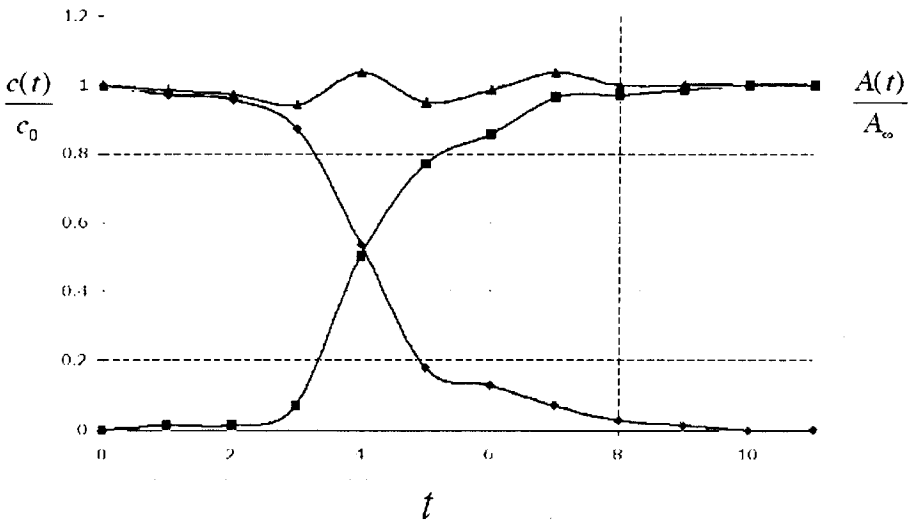

Figure 6: Characteristic experimental results for relative monomer concentration, $c(t)/c_o$ (diamond), mass in fibril, $A(t)/A_\infty$ (squares), and the sum of the two data sets, $c(t)/c_o + A(t)/A_\infty$ (triangles) versus time (horizontal axis). The sum suggests that most monomer mass is present in either fibril or monomer form throughout fibrillogenesis of hIAPP. This graph was extrapolated from results presented by Miranker and Ruschak (6).

9.6 Nucleation Dependent Model

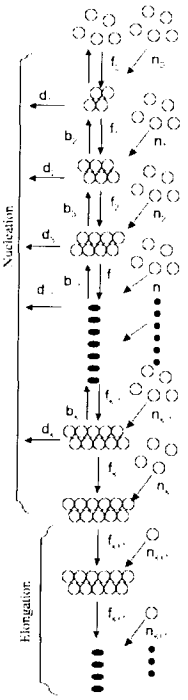

Figure 7: Generic nucleation dependent model, the basic model that describes the nucleated polymerization of a self assembling polymer. Monomers are assumed to quickly associate and dissociate to form short lived oligomers. These oligomers are assumed to quickly come into steady state with the monomer population. Stable nuclei are then formed on a slower time scale and quickly elongate to form polymers.

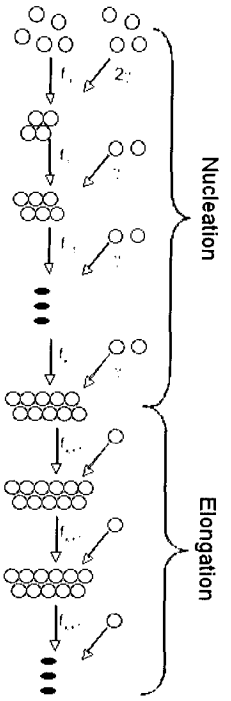

Figure 8: Schematic of the scaled generic nucleation-dependent model as determined for hIAPP fibril formation. This figure represents the only possible subset of the nucleation dependent polymerization model that is consistent with the observation that the fluorescence profiles generated from various initial monomer concentrations of hIAPP scale systematically to produce a single curve, implying that the initial monomer concentration is immaterial to the formation kinetics of hIAPP fibrils.

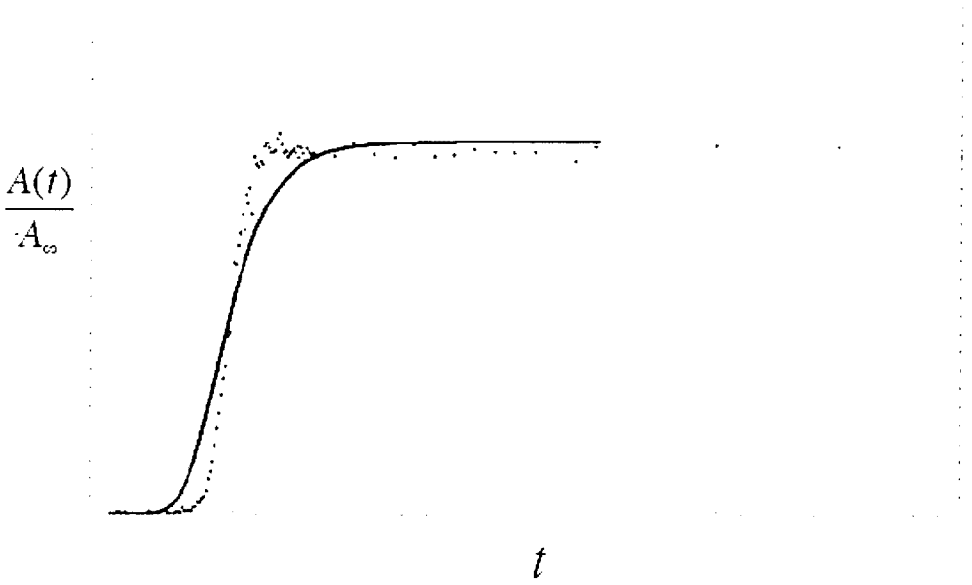

Figure 9: Characteristic fit for the time-dependent behavior of scaled fluorescence, $A(t)/A_\infty$ (vertical axis) versus time (horizontal axis), of hIAPP to the scaled single nucleation dependent polymerization model. This fit exemplifies the inability of the NDP model to capture the rapid rise-time seen in the fluorescence, after the pronounced lag phase. Thus we have elucidated the fact that no version of the nucleation dependent polymerization model will accurately describe the fibrillogenesis of hIAPP, given the observation that initial monomer concentration is not relevant to the fluorescence profile generated for the formation of hIAPP fibrils under systematic scaling.

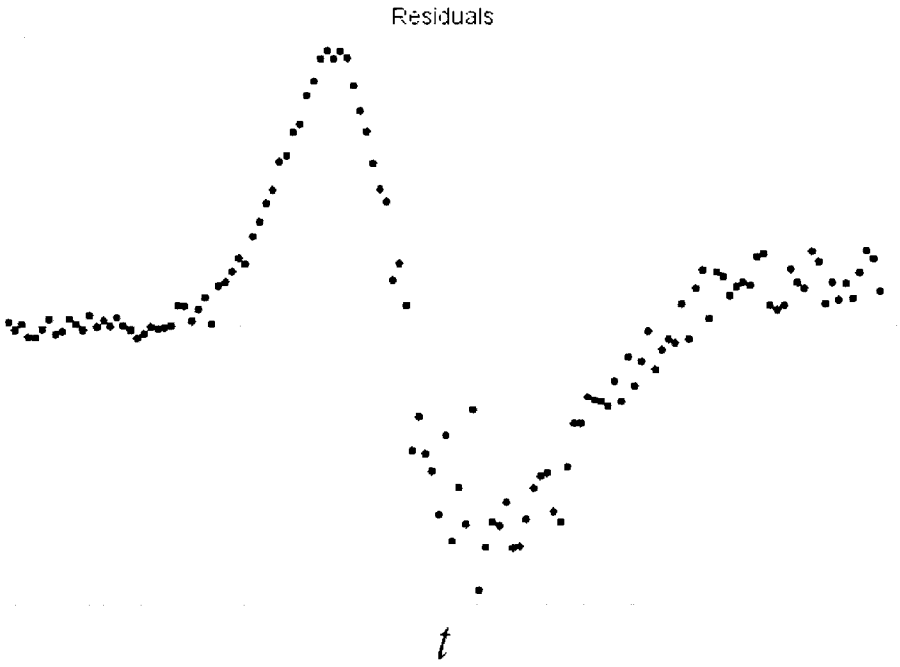

Figure 10: Representative residuals of the best fits of scaled experimental fluorescence $A(t)/A_\infty$, Figure (9), to the single nucleation dependent polymerization model. This result implies a systematic failure of the generic NDP model to accurately capture the fluorescence data for hIAPP.

9.7 The Three Stage Model of Amyloid Fibril Formation

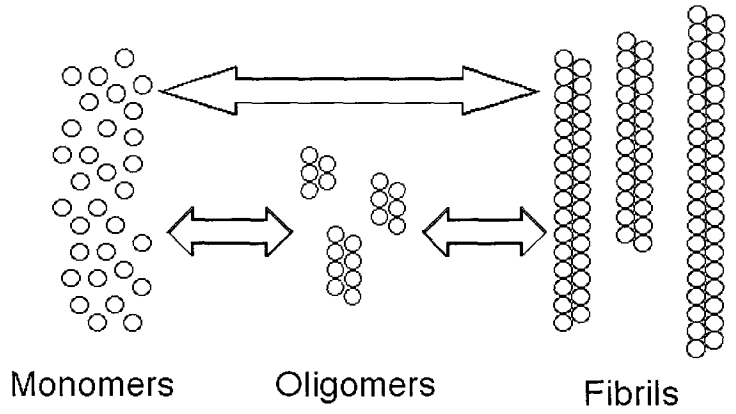

Figure 11: The three stage model of amyloid fibril formation, as proposed by Chaung-Chung Lee (2007). This model allows unstable oligomers to assemble by monomer addition at each stage until an unstable nucleus is created. Unstable fibrils then form by monomer addition to nuclei and may grow by addition of monomers or oligomers of any size.

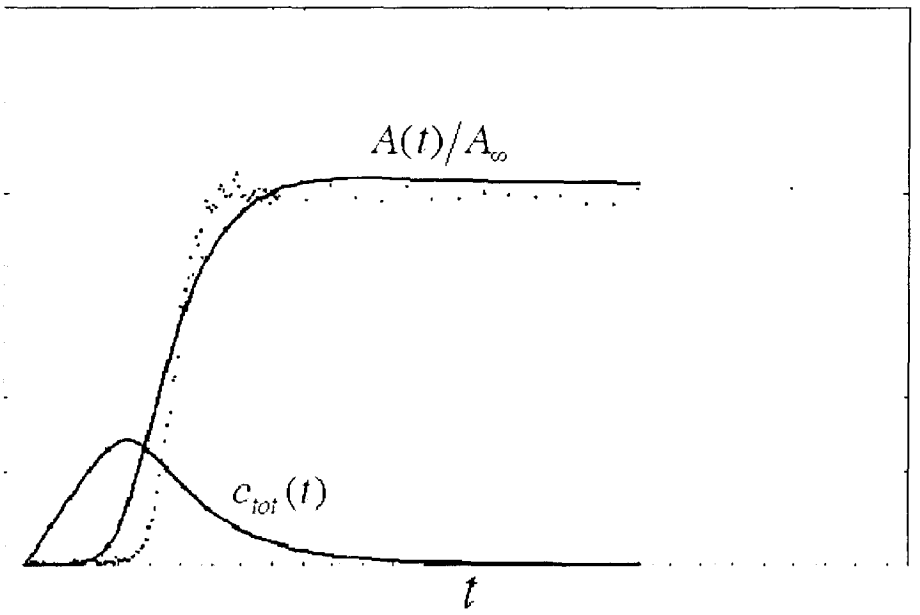

Figure 12: Typical best fit of monomer in fibril and corresponding total oligomer population (vertical axis) for the three stage model of amyloid fibril formation, versus time (horizontal axis). In this model fibrils are allowed to elongate through both monomer and oligomer addition to fibril ends. While this model obeys both our scaling and the artificial power law given by $\gamma = 1$, it does not support the observation of persistent oligomers for non trivial oligomer-fibril elongation rates. Furthermore, elongation kinetics do not support a theory of fibril elongation through oligomer addition for hIAPP.

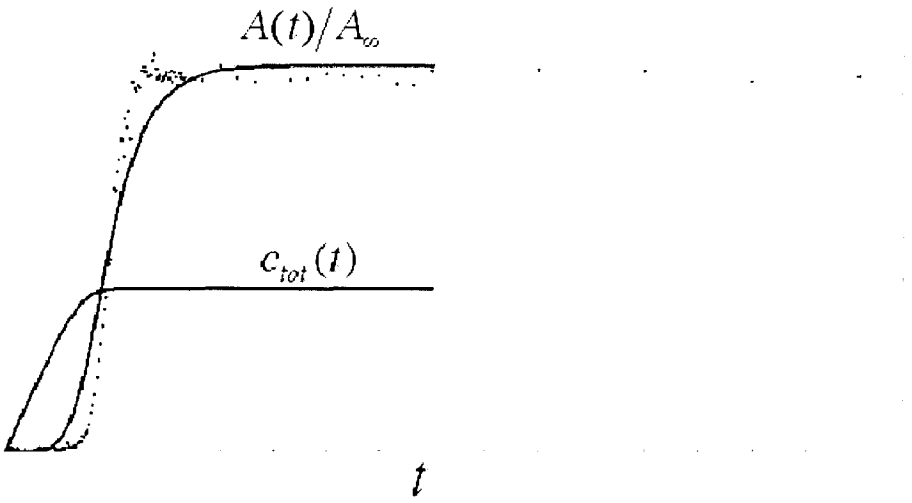

Figure 13: Typical best fit of monomer in fibril and corresponding total oligomer population (vertical axis) for the three stage model of amyloid fibrillation without fibril elongation through oligomer addition, versus time (horizontal axis). While this model obeys both a scaling and power law, and supports the observation of persistent oligomers, it reduces to the NDP model with the imposed scaling $\gamma = 1$.

9.8 Nucleation Dependent Model With Off-Pathway Aggregates

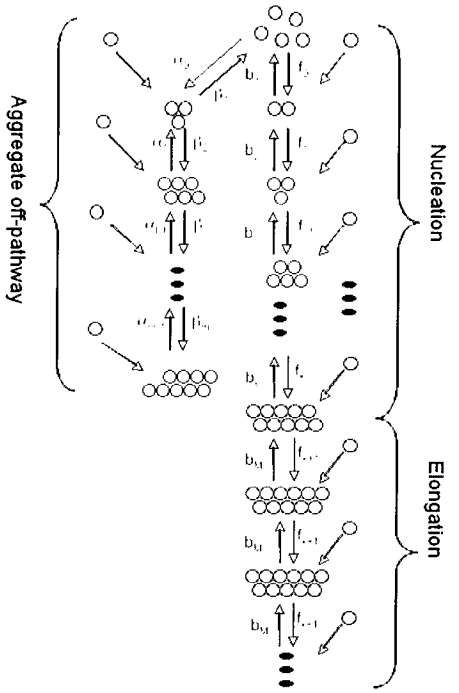

Figure 14: Schematic for the NDP model with off-pathway kinetics of aggregation, as proposed by Powers (30). Oligomers, as well as aggregates, are allowed to form by addition of a monomer at each step in the formation process. However, aggregate and oligomer formation are only allowed to "communicate" information through the monomer pool. This model has been proposed to account for the persistent oligomer / aggregate population observed alongside growing and mature fibrils.

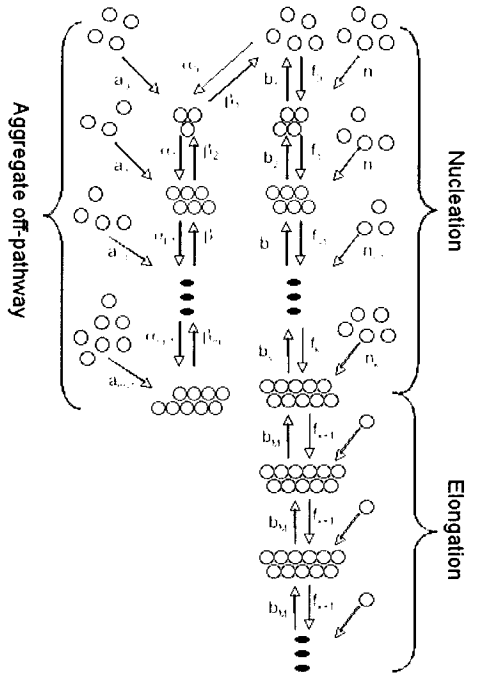

Figure 15: Generic NDP model with off-pathway kinetics. This is a generalization of the model proposed by Powers (30) where oligomers, as well as aggregates, are allowed to form by addition of any number of monomers at any step in the formation process. However, aggregation and oligomer formation are only allowed to "communicate" information through the monomer pool.

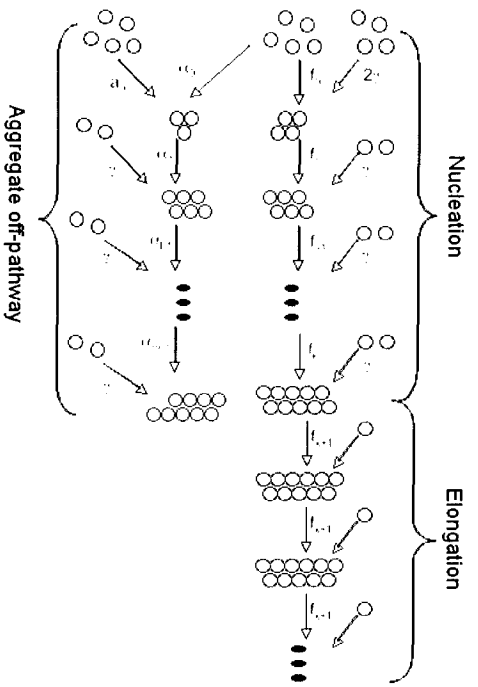

Figure 16: Generic NDP model with off-pathway aggregates as restricted by the scaling and the power law observed from fluorescence data of hIAPP fibril formation. Here we see that aggregates are restricted in the same way as oligomers and grow by the same number of monomers at each step of assembly, except for perhaps the first aggregate species. Furthermore, we see that aggregate populations are only allowed to grow at a non trivial rate, implying that aggregates cannot act as a buffer to the monomer concentration at "large" initial concentrations.

9.9 Nucleation Dependent Model With Fibril Dependant Secondary Nucleation

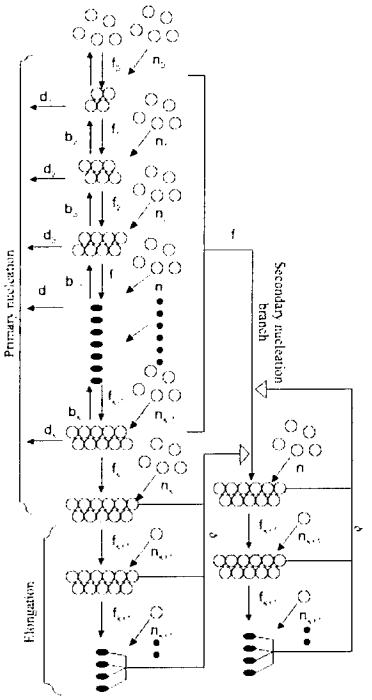

Figure 17: Generic nucleation dependent model with fibril-dependent secondary nucleation. This figure represents a nucleation dependent polymerization process that is facilitated by a second nucleation step which is fibril dependent. This additional nucleation step has been proposed to address the inability of the nucleation dependent polymerization model to describe the fibrillogenesis of hIAPP as observed with a Th-T assay. The secondary nucleation process could include branching, breaking, or surface mediated nucleation. We allow the data to "suggest" the most probable candidate for secondary nucleation.

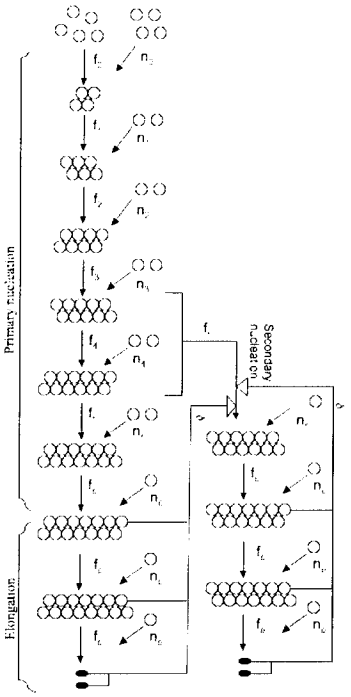

Figure 18: Assembly kinetics of hIAPP as discerned from phenomenological modeling of nucleated polymer formation of the generic nucleation dependent model with fibril-dependent secondary nucleation. This figure shows that nuclei are formed in five steps. First, four monomers combine to form the first oligomer c_1, then two monomers bind to c_1 forming c_2. This addition of monomer pairs continues until c_4, after which a stable nucleus of twelve monomers is formed from c_4 by addition of two monomers. Fibrils then grow by unit addition. As fibrils form, a secondary fibril dependent nucleation occurs by addition of a single monomer to the c_4 species. These secondary nuclei then form fibrils by unit addition.

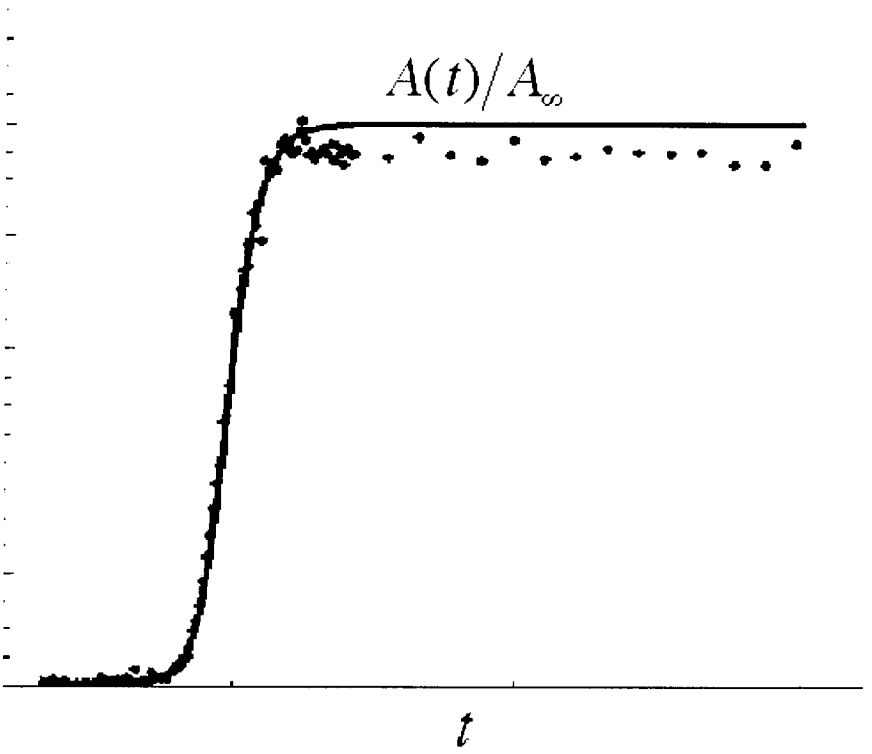

Figure 19: Characteristic fit for the nucleation dependent polymerization model with secondary fibril surface mediated nucleation, as derived from the phenomenological model of the fluorescence profile corresponding to monomer of human islet polypeptide in fibril mass over time. The predictions from the unique model, as determined by systematic scaling and application of the corresponding power law, suggest our phenomenological theory is in excellent agreement with the data up until maximum fluorescence is reached for all observed initial concentrations of monomers observed.

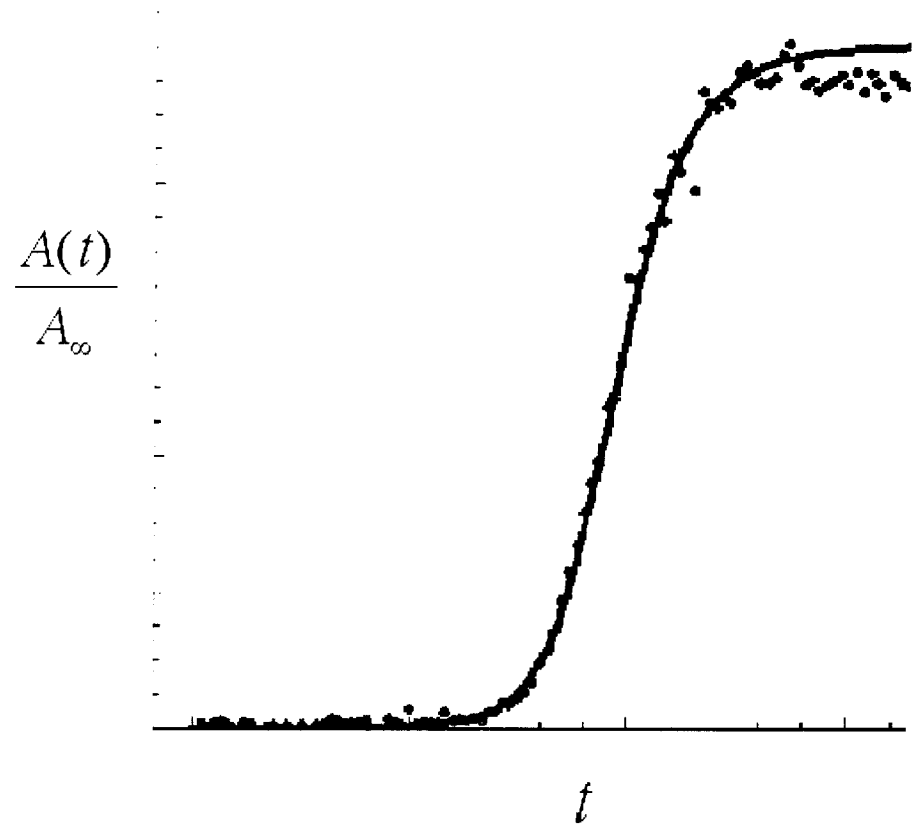

Figure 20: A closer view of the lag and elongation phases of fibril formation fluorescence. Here we see our phenomenological model of nucleation dependent polymerization with secondary fibril surface mediated nucleation captures both the rapid transition from lag phase to fibril elongation, as well as, the rapid exponential decrease in fluorescence, corresponding to an exponential decrease in fibril formation.

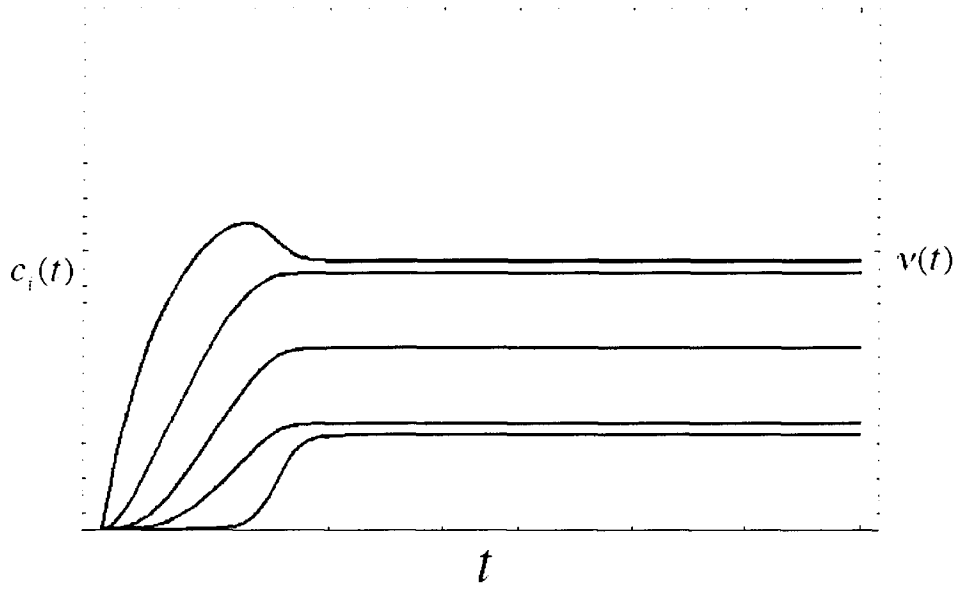

Figure 21: Theoretical oligomer and nuclei populations formed during the fibrillogenesis of human islet amyloid polypeptide as predicted by the scaled nucleation dependent model of fibril formation with secondary surface mediated nucleation. c_1, c_2, c_3, c_4, and nuclei top to bottom, respectively.

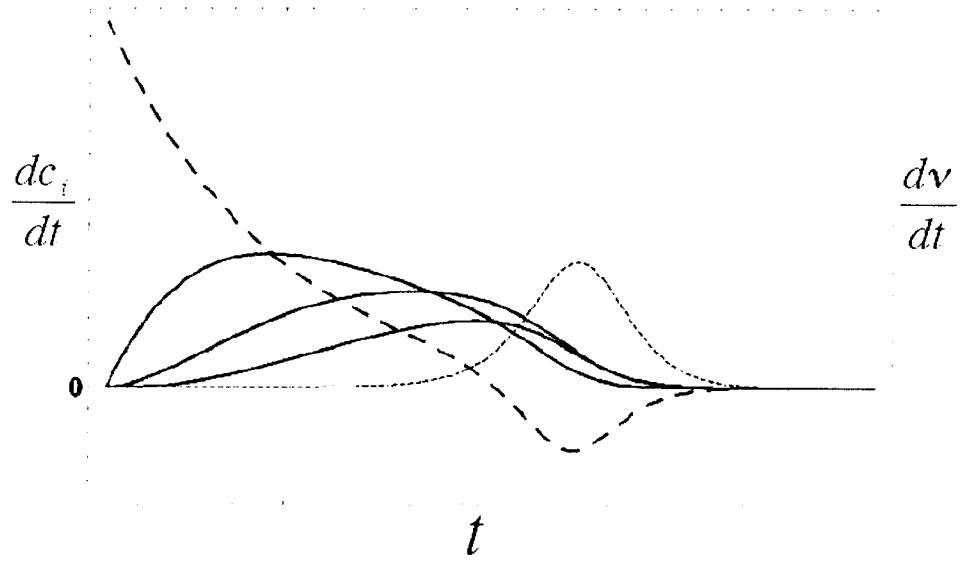

Figure 22: Theoretical formation rates of oligomer and nuclei populations formed during the fibriogenesis of human islet amyloid polypeptied as predictied by the scaled nucleation dependant model of fibril formation with secondary surface mediated nucleation. c_1, bold dsahed, c_2, c_3, c_4, solid line, top to bottom respectively, and nuclei, dashed.

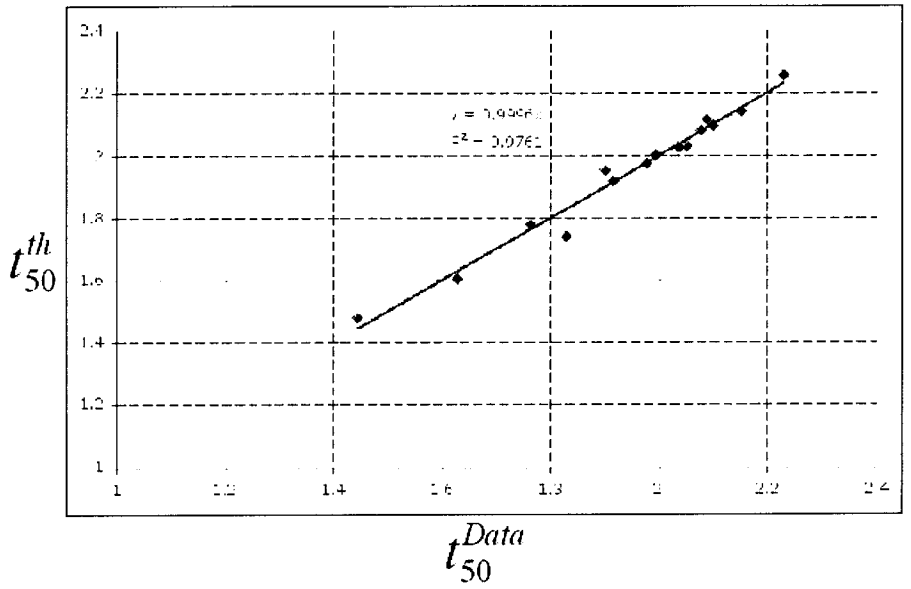

Figure 23: Theoretical values of the time to 50% completion t_{50}^{th} (vertical axis) vs. experimental time to 50% completion t_{50}^{data} (horizontal axis).

9.10 Elongation Kinetics

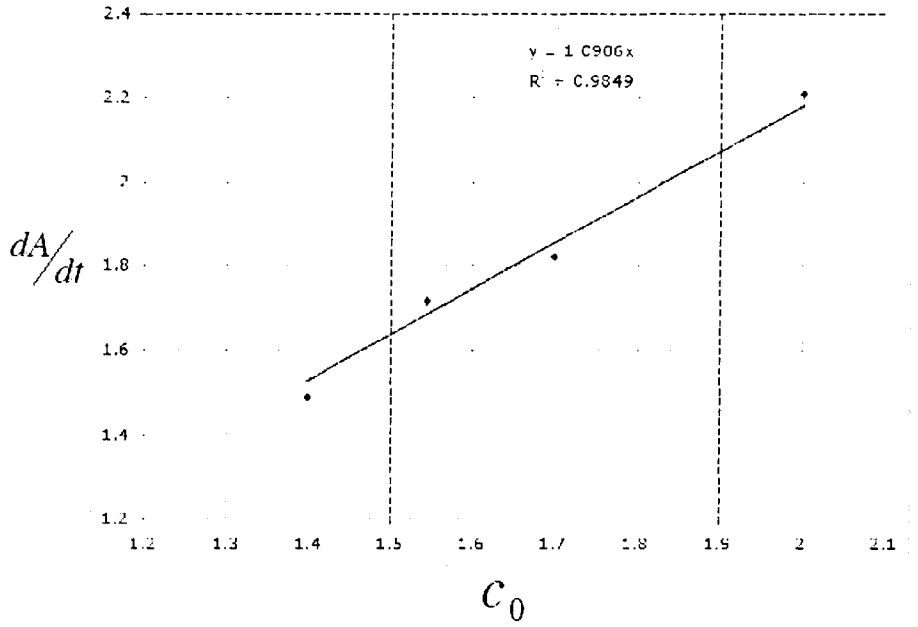

Figure 24: Log Log plot of the slope of elongation fluorescence (vertical axis) as read from Figure (4) vs. initial monomer concentration of hIAPP added to seeded reactions (vertical axis). Here we see the slope of the best fit line is approximately 1, suggesting that elongation of fibrils is due to monomer addition.

9.11 Length Distribution

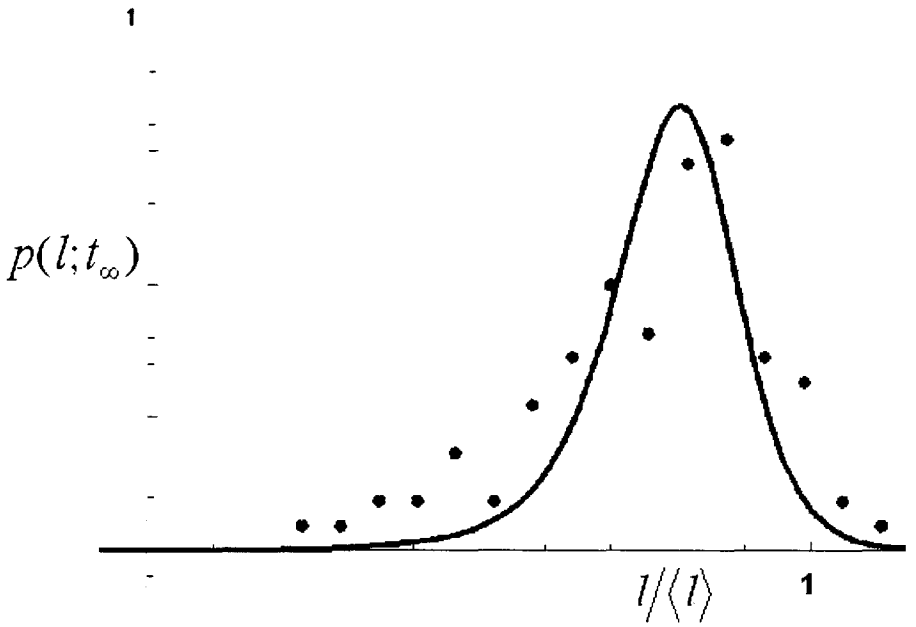

Figure 25: Predictions for normalized fibril length distribution of the nucleation dependent polymerization model with secondary fibril dependent surface mediated nucleation, based on scaled fluorescence data, solid line, plotted with experimental fibril length distribution, dots.

9.12 Parameter Variations

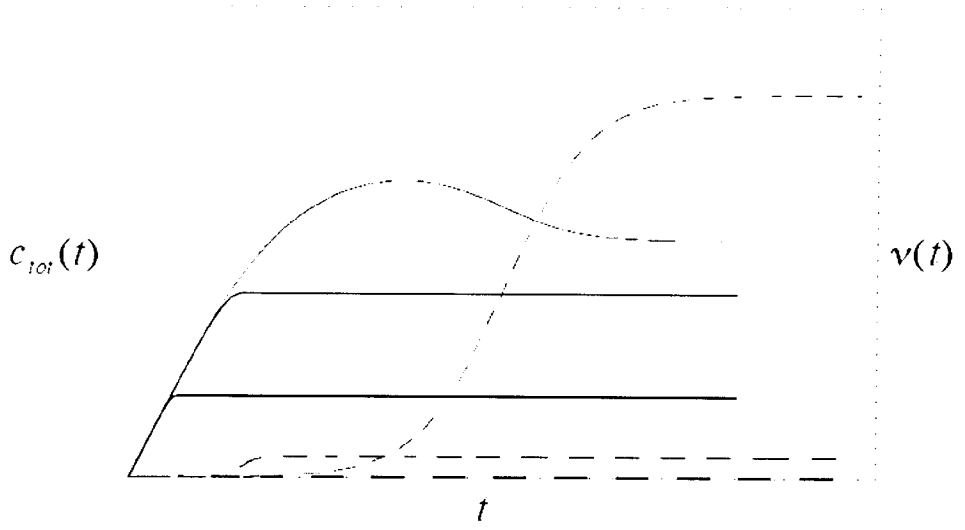

Figure 26: Effects of altering fibril elongation rates on number of fibrils (dashed) and total oligomer populations (solid). This chart shows as elongation rates increase total number of fibrils present decreases. Furthermore, the total oligomer populations also monotonically decrease with increasing elongation rates. Here increased elongation rates correspond to thicker plot lines. Thus, according to our model, acceleration of fibril formation kinetics will result in fewer, longer fibrils and a lower total oligomer population throughout fibrillogenesis. This implies less cytotoxicity for accelerated fibril elongation and a dramatic increase in potentially toxic oligomer and fibril densities for retarded fibril elongation kinetics.

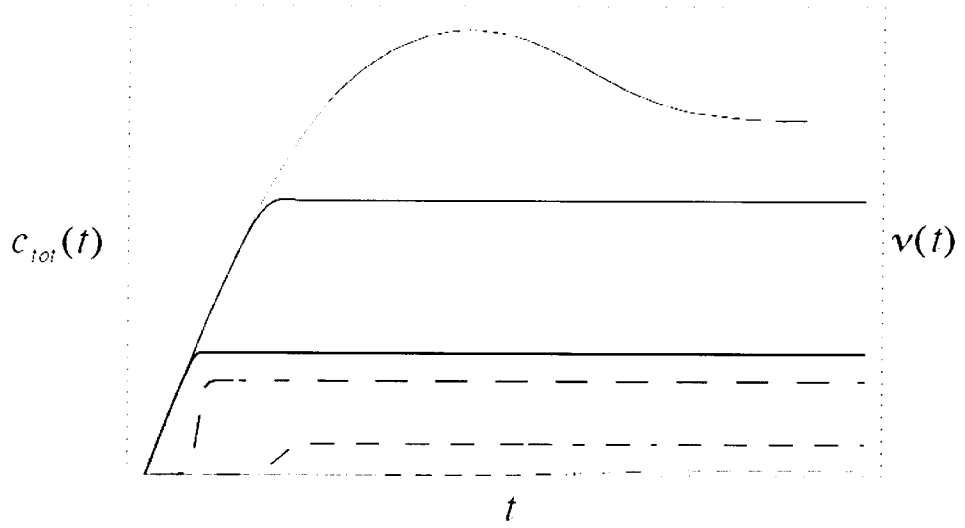

Figure 27: Effects of altering fibril nuclei formation rates on number of fibrils (dashed) and total oligomer populations (solid). This chart shows as nucleation rates increase total number of fibrils present increase. However, the total oligomer populations are predicted to monotonically decrease with increasing nucleation rates. Here increased nucleation rates correspond to thicker plot lines. Thus, according to our model, acceleration of fibril nuclei formation kinetics will result in increasing fibril numbers of shorter lengths, but a lower total oligomer population throughout fibrillogenesis. This implies greater cytotoxicity for accelerated fibril nucleation, should fibril density increase cytotoxicity. Conversely, a dramatic increase in potentially toxic oligomer is seen for retarded fibril nucleation kinetics.

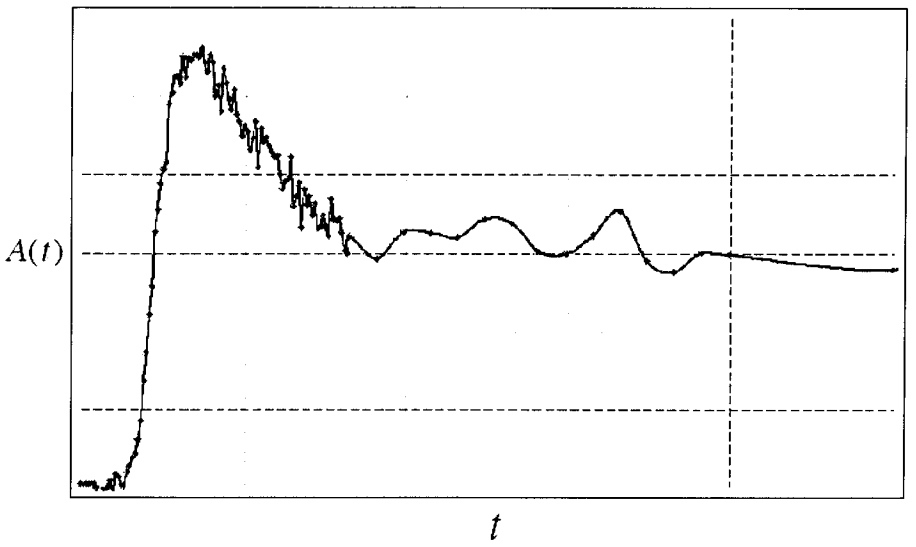

Figure 28: Fluorescence data for heparin. Note the drop in Fluorescence after maximum fluorescence has been reached. This drop implies that fibril may catastrophe, a feature beyond the scope of the model presented here. Furthermore, various initial concentrations of hIAPP do not scale for a given heparin concentration. Thus, we conclude that heparin amplifies the hitherto trivially small reverse rates, which we have scaled out of our model.

9.13 Scaling Violation

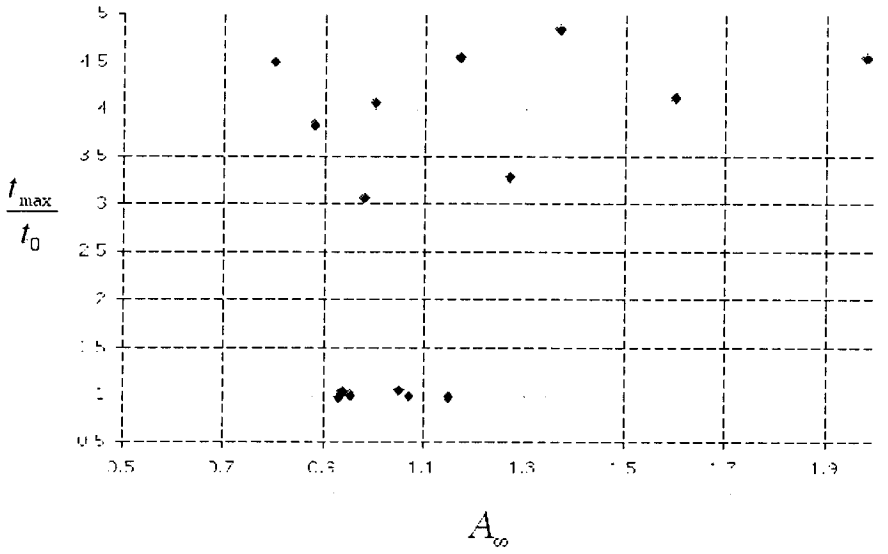

Figure 29: Plot of t_{max}/t_o vs. A_∞. This plot reveals that out scaling is not perfect. For perfectly scalable data t_{max}/t_o would be constant and not dependent on A_∞. Thus we see, for later times that our approximation is inconsistent with the observed data.

10 Bibliography

1. Dominique P., Terrell H., Marie C., Edward K. 1985 A model for actin polymerization and the kinetic effects of ATP hydrolysis. Proc. Natl. Acad. Sci. USA 82(21):7207-7211

2. Oosawa, F., and S. Asakura. 1975 Thermodynamics of the polymerization of protein. Academic Press, London.

3. Flyvbjerg H., Jobs E., Leibler, S. 1996 Kinetics of self-assembling microtubules: An inverse problem in biochemistry. Proc. Natl. Acad. Sci. USA 93:5975-5979.

4. Claude B., Nicole B., Benjamin L., Marie-Ccile H., and Christian L., 2007 Kinetic analysis of tubulin assembly in the presence of the microtubule-associated protein TOGp. J Biol Chem. 282(8):5570-5581.

5. Ferrone F. 1999 Analysis of protein aggregation kinetics. Methods Enzymol. 309:256-274.

6. Amy M. R., Andrew D. M. 2007 Fiber-dependent amyloid formation as catalysis of an existing reaction pathway Proc. Natl. Acad. Sci. USA 104:12341-12346

7. Cristian Ionescu-Zanetti, Ritu K. 1999 Monitoring the assembly of Ig light-chain amyloid fibrils by atomic force microscopy. Proc. Natl. Acad. Sci. USA 6(23):13175-13179.

8. Rebecca L. H., Gunilla T. W., Per W., Steven E. K. 2004 Islet Amyloid: A Crtical Entity in the Pathogenesis of Type 2 Diabetes. Clinical Endocrinology and Metabolism 89(8):3629-3643

9. Tan S. Y., Pepys M. B. 1994 Amyloid. Histopathology 25:403-413

10. Westermark P., Benson MD., Buxbaum J. N., Choen A. S., Frangione B., Ikeda S., Masters C. L., Merilin G., Saraiva M. J., Sipe JD. 2002 Amyloid fibril protein nomenclature. Amyloid 9:197-200

11. Glenner G. G., Wong C. W. 1984 Alzheimer's disease initial report of the initialtion and purafacation of a novev cyrebrovasculer amyloid protein. Biochem Biophys Res Commun. 120:885-890

12. Glenner G. G., Wong C. W., Quaranta V., Eanes E. D. 1984 The amyloid deposits

in Alzheimer's disease: their nature and pathogenesis. Apply Pathology 2:357-369

13. Masters CL., Simms G., Weinman N. A., Multhaup G., McDonald B. L., Beyreuther K. 1985 Amyloid plaque core protein in Alzheimer disease and Down syndrome. Proc Natl Acad Sci USA 82:4245-4249

14. Opie L. 1901 The relationship of diabites Millitus to lessions of the pancrease: hyaline degeneration of the islets of Langerhans. J Exp Med 5:527-540

15. Westermark P., Wernstedt C., Wilander E., Hayden D. W., OBrien T. D., Johnson K. H. 1987 Amyloid fibrils in human insulinoma and islets of Langerhans of the diabetic cat are derived from a neuropeptide-like protein also present in normal islet cells. Proc Natl Acad Sci USA 84:3881-3885

16. Westermark P., Wernstedt C., Wilander E., Sletten K. 1986 A novel peptide in the calcitonin gene related peptide family as an amyloid fibril protein in the endocrine pancreas. Biochem Biophys Res Commun 140:827-831

17. Cooper G. J. S., Willis A. C., Clark A., Turner R. C., Sim R. B., Reid K. M. 1987 Purification and characterization of a peptide from amyloid-rich pancreases of type 2 diabetic patients. Proc Natl Acad Sci USA 84:8628-8632

18. Kahn S. E., D Alessio D. A., Schwartz M. W., Fujimoto W. Y., Ensinck J. W., Taborsky G. J., Porte Jr. D. 1990 Evidence of co-secretion of islet amyloid polypeptide and insulin by. βcells. Diabetes 39:634 -638

19. Butler P. C., Chou J., Carter W. B., Wang Y. N., Bu B. H., Chang D., Chang J. K., Rizza R. A. 1990 Effects of meal ingestion on plasma amylin concentration in NIDDM and non-diabetic humans. Diabetes 39:752-756

20. Hartter E., Svoboda T., Ludvik B., Schuller M., Lell B., Kuenburg E., Brunn bauer M., Woloszczuk W., Prager R. 1991 Basal and stimulated plasma levels of pancreatic amylin indicate its co-secretion with insulin in humans. Dia betologia 34:52-54

21. Kahn S. E., Fujimoto W. Y., DAlessio D. A., Ensinck J. W., Porte Jr. D. 1991 Glucose stimulates and potentiates islet amyloid polypeptide secretion bt te βcells Horm Metab Res 23:577-580

22. Enoki S., Mitsukawa T., Takemura J., Nakazato M., Aburaya J., Toshimori H., Matsukara S. 1992 Plasma islet amyloid polypeptide levels in obesity, impaired glucose-tolerance and non-insulin-dependent diabetes-mellitus. Diabetes Res Clin Pract 15:97-102

23. Kautzky-Willer A., Thomaseth K., Pacini G., Clodi M., Ludvik B., Streli C. Waldhausl W., Prager R. 1994 Role of islet amyloid polypeptide secretion in insulin resistant humans. Diabetologia 37:188-194

24. Thomaseth K., Kautzky-Willer A., Ludvik B., Prager R., Pacini G. 1996 Integrated mathematical model to assess βcell activity during the oral glucose test. Am J Physiol 33:E522-E53

25. Rabkin R., Reaven G. M., and Mondon C. E. 1986 Insulin metabolism by liver, muscle, and kidneys from spontaneously diabetic rats. AJP - Endocrinology and Metabolism 250 (5):530-E537

26. Dechenes CJ., Verchere CB., Andrikopoulos S., Kahn SE. 1998 Human aging is associated with parallel reductions in insulin and amylin release. Am J Physiol 38:E785-E791

27. Kahn S. E., Verchere C. B., Andrikopoulos S., Asberry P. J., Leonetti D. L., Wahl P. W., Boyko E. J., Schwartz R. S., Newell-Morris L., Fujimoto W. Y. 1998 Reduced amylin release is a characteristic of impaired glucose tolerance and type 2 diabetes in Japanese Americans. Diabetes 47:640-645

28. Knowles N. G., Landchild M. A., Fujimoto W. Y., Kahn S. E. 2002 Insulin and amylin release are both diminished in first-degree relatives of subjects with type 2 diabetes. Diabetes Care 25:292-297

29. Novials A., Sarri Y., Casamitjana R., Rivera F., Gomis R. 1993 Regulation of islet amyloid polypeptide in human pancreatic islets. Diabetes 42:1514-1519

30. Kautzky-Willer A., Thomaseth K., Ludvik B., Nowotny P., Rabensteiner D., Waldhausl W., Pacini G., Prager R. 1997 Elevated islet amyloid pancreatic polypeptide and proinsulin in lean gestational diabetes. Diabetes 46:607-614

31. Hall D., Edskes H. 2004 Silent prions lying in wait: a two-hit model of prion/amyloid formation and infection. J. Mol. Biol. 336:775-786.

32. Tanaka M., Craparo E. F., Martorana V., Bulone D., San Biagio P. L. 2006 The physical basis of how prion conformations determine strain phenotypes. Biophys J 90:4585-4591

33. Chuang-Chung L., Arpan N., Ananthakrishnan S., Georges B., and Gregory J., 2007 A Three-Stage Kinetic Model of Amyloid Fibrillation. Biophysical Journal 92:3448-

3458.

34. Lucy M., Christopher J. R., Donald F. S., Leena H., Philippe A. H., Bruce V. 2006 Impaired NH2-Terminal Processing of Human Proislet Amyloid Polypeptide by the Prohormone Convertase PC2 Leads to Amyloid Formation and Cell Death. Diabetes 55, 2192-2201.

35. Porat Y., Kolusheva S., Jelinek R., Gazit E. 2003 The human islet amyloid polypeptide forms transient membrane-active prefibrillar assemblies. Biochemistry 42:10971-10977

36. Evan T. P., David L. P. 2008 Mechanisms of protein fibril formation: Nucleated polymerization with competing off-pathway aggregation 94:379-391

37. Leighton B., Cooper G. J. S. 1988 Pancreatic amylin and calcitonin gene-related peptide cause resistance to insulin in skeletal-muscle in vitro. Nature 335:632-635

38. Sowa R., Sanke T., Hirayama J., Tabata H., Furuta H., Nishimura S., Nanjo K. 1990 Islet amyloid polypeptide amide causes peripheral insulin resistance *in-vivo* dogs. Diabetologia 33:118-120

39. Chance W. T., Balasubramaniam A., Zhang F. S., Wimalawansa S. J., Fischer J. E. 1991 Anorexia following the intrahypothalamic administration of amylin Brain Res 539:352-354

40. Chance W. T., Balasubramaniam A., Stallion A., Fischer J. E. 1993 Anorexia following the systemic injection of amylin. Brain Res 607:185-188

41. Lutz T. A., Senn M., Althaus J., DelPrete E., Ehrensperger F., Scharrer E. 1998 Lesion of the area postrema nucleus of the solitary tract (AP/NTS) attenuates the anorectic effects of amylin and calcitonin gene-related peptide (CGRP) in rats. Peptides 19:309 -317

42. Arnelo U., Herrington M. K., Theodorsson E., Adrian T. E., Reidelberger R., Larsson J., Marcusson J., Strommer L., Ding X., Permert J. 2000 Effects of long-term infusion of anorexic concentrations of islet amyloid polypeptide on neurotransmitters and neuropeptides in rat brain. Brain Res 887:391-398

43. Wookey P. J., Tikellis C., Du. H. C., Qin H. F., Sexton P. M., Cooper M. E. 1996 Amylin binding in rat renal-cortex, stimulation of adenylyl-cyclase, and activation of plasma-renin. Am J Physiol 39:F289 -F294

44. Chai S. Y., Christopoulos G., Cooper M. E., Sexton P. M. 1998 Characterization of binding sites for amylin, calcitonin, and CGRP in primate kidney. Am J Physiol 43:F51-F62

45. Gilbey S.G., Ghatei M. A., Bretherton-Watt D., Zaidi M., Jones P. M., Perera T., Beacham J., Girgis S., Bloom S. R. 1991 Islet amyloid polypeptide: production by an osteoblast cell-line and possible role as a paracrine regulator of osteoclast function in man. Clin Sci 81:803-808

46. Alam A., Moonga B. S., Bevis P. JR., Huang C. L. H., Zaidi M. 1993 Amylin inhibits bone-resorption by a direct effect on the motility of rat osteoclasts. Exp Physiol 78:183-196

47. Westermark P., Eizirik D. L., Pipeleers D. G., Hellerstrom C., Andersson A. 1995 Rapid deposition of amyloid in human islets transplanted into nude mice. Diabetologia 38:543-549

48. Westermark G., Westermark P., Eizirik D. L., Hellerstrom C., Fox N., Steiner D. F., Andersson A. 1999 Differences in amyloid deposition in islets of transgenic mice expressing human islet amyloid polypeptide versus human islets implanted into nude mice. Metab Clin Exp 48:448-454

49. Porte Jr. D., Kahn S. E. 1989 Hyperproinsulinemia and amyloid in NIDDM: clues to etiology of islet β-cell dysfunction? Diabetes 38:1333-1336

50. Charge S. B. P., de Koning E. J. P., Clark A. 1995 Effect of pH and insulin on fibrillogenesis of islet amyloid polypeptide in-vitro. Biochemistry 34:14588-14593

51. Westermark P., Li Z. C., Westermark G. T., Leckstro A., Steiner D. F. 1996 Effects of β-cell granule components on human islet amyloid polypeptide fibril formation. FEBS Lett 379:203-206

52. Hegyi P., Rakonczay Z., Gray M., Argent B., 2004 Measurement of Intracellular pH in Pancreatic Duct Cells: A New Method for Calibrating the Fluorescence Data. Pancreas. 28(4):427-434.

53. Peter M., Andisheh A. 2007 Aromatic Interactions Are Not Required for Amyloid Fibril Formation by Islet Amyloid Polypeptide but Do Influence the Rate of Fibril Formation and Fibril Morphology. Biochemistry 46(11):1731-1418.

54. Kayed R., Head E., Thompson JL., McIntire TM., Milton SC., Cotman CW., Glabe CG. 2003 Common structure of soluble amyloid oligomers implies common mechanism of pathogenesis. Science 300:486-489

55. Shae B., Padrik M., Andrew M. 2002 Islet Amyloid: Phase Partitioning and Secondary Nucleation Are Central to the Mechanism of Fibrillogenesis. Bioghemistry 41: 4694-4703

56. Harrey LeVine III 1999 Quantification of β-Sheet Amyloid Fibril Structure with Thioflavin T. Methods in Enzymology 309:274-284

11 Appendix

11.1 Scaled Data Collapse

The observed similar shape in the time series fluorescence data motivates the question: Do the observed data sets differ only by a characteristic scale in fluorescence and time? Mathematically we ask whether the observed data sets could be described by a single function, such as

$$A(t; A_\infty) = A_\infty f[t/t_0(A_\infty)], \quad [1]$$

where f is dimensionless. To determine if the data is described by Eq.(1) we let

$$g(t') = \log[f(10^{t'})].$$

We may now write Eq.(1) as

$$\log[A] = g[\log(t) - \log(t_0)] + \log[A_\infty]. \quad [2]$$

If Eq.(2) is satisfied we may say that the observed fluorescence data only differs by horizontal and vertical shifts of $\log[t_0]$ and $\log[A_\infty]$, respectively. Therefore, the kinetics have no dependence on c_0, the initial monomer concentration. Figure(2) shows this to be approximately true for our data. We now look for a relationship between A_∞ and t_0. Values of t_0 are readily determined from plots of A/A_∞ vs. t. These values are plotted against the corresponding values of A_∞ on a log-log plot in Figure(3). Fitting a linear function gives the approximate relationship

$$t_0 \propto A_\infty^{-\gamma},$$

with

$\gamma = 2$ over the entire range of initial monomer concentrations assayed here.

11.2 NDP Model reduction

From section[6.1] we observe that substituting the scaling variables into the model gives

$$\frac{d\hat{c}_1}{dt} = \lambda[\frac{f_0 c_0^{n_0-\gamma}\hat{c}^{n_0}}{X} - f_1 c_0^{n_1-\gamma}\hat{c}^{n_1}\hat{c}_1 + \hat{c}_0^{-\gamma}(b_2\hat{c}_2 - d_1\hat{c}_1)],$$

$$\frac{d\hat{c}_i}{dt} = \lambda[f_{i-1}\hat{c}^{n_{i-1}}c_0^{n_{i-1}-\gamma}\hat{c}_{i-1} - f_i\hat{c}^{n_i}c_0^{n_i-\gamma}\hat{c}_i + \hat{c}_0^{-\gamma}(-b_i\hat{c}_i + b_{i+1}\hat{c}_{i+1} - d_i\hat{c}_i)], \quad \text{for } 2 \leq i \leq k.$$

Furthermore we have

$$\frac{d\hat{\nu}}{dt} = \frac{\lambda X}{\mu}[f_k\hat{c}^{n_k}c_0^{n_k-\gamma}\hat{c}_k],$$

$$\frac{d\hat{M}}{dt} = \mu\lambda[f_{k+1}\hat{c}_0^{-\gamma}\hat{c}\hat{\nu}].$$

We now let

$$\mu = c_0^{\gamma},$$

$$X = \mu,$$

$$n_i = \gamma, \quad \text{for } 1 \leq i \leq k,$$

and

$$n_0 = 2\gamma.$$

Substituting these values into the equations results in

$$\frac{d\hat{c}_1}{dt} = f_0\hat{c}^{2\gamma} - f_1\hat{c}^{\gamma}\hat{c}_1 + \hat{c}_0^{-\gamma}(b_2\hat{c}_2 - d_1\hat{c}_1),$$

$$\frac{d\hat{c}_i}{dt} = f_{i-1}\hat{c}^{\gamma}\hat{c}_{i-1} - f_i\hat{c}^{\gamma}\hat{c}_i + \hat{c}_0^{-\gamma}(-b_i\hat{c}_i + b_{i+1}\hat{c}_{i+1} - d_i\hat{c}_i), \quad \text{for } 2 \leq i \leq k.$$

Likewise we have

$$\frac{d\hat{\nu}}{dt} = f_k\hat{c}^{\gamma}\hat{c}_k,$$

and

$$\frac{d\hat{M}}{dt} = f_{k+1}\hat{c}\hat{\nu}.$$

Removal of the remaining explicit terms in c_0 is accomplished by setting

$$(b_{i+1}\hat{c}_{i+1} - b_i\hat{c}_i - d_i\hat{c}_i) = 0,$$

and

$$(b_2\hat{c}_2 - d_1\hat{c}_1) = 0.$$

Thus we have determined that neither the off-rates, b_i, nor the disintegration rates, d_i, are relevant to the kinetics and no net flux of monomers into or out of the various oligomer species exist due to these terms.

11.3 The Three Stage Model of Amyloid Fibrillation

Here we present a systematic scaling of the model by Chaung-Chung Lee and others (33). We will show under the condition of data collapse as observed for hIAPP that the model reduces to the scaled NDP model where Chaung-Chung Lee have artificially enforced a scaling law of the form,

$$t_0 \propto A_\infty^{-\gamma}, \qquad \text{for } \gamma = 1.$$

From Figure (11) and section [6.2] we may write differential equations for the formation of fibrils from an unstructured monomer pool. This model allows for the formation of oligomers by the addition of one monomer at each step of oligomer formation. Furthermore, the growth and decay of fibrils is allowed by the addition or removal of any size oligomer from fibril ends. The original model by (33) tracks density of fibrils. This term parallels the density of nuclei in the NDP model, and does not track total monomer mass in fibril. However this quantity is easily discerned with the model and is included in this analysis for easy comparison to observed fluorescence profile of hIAPP. The model by Chaung-Chung Lee assumes monomers begin as properly folded hexamers which irreversibly form monomers. Here we have assumed an initial monomer concentration. This modification will have no impact on the observations presented here. The original model of Chaung-Chung Lee, given the assumptions and modifications above, is

$$\frac{dc}{dt} = -f_{k+1} c F + s_o F.$$

Here we have again assumed the mass of monomers is predominantly contained in monomers and fibrils. Furthermore, we have

$$\frac{dc_1}{dt} = f_0 c^2 - f_1 c_1 c + b_2 c_2 - b_1 c_1 + s_1 F - l_1 c_1 F,$$

$$\frac{dc_i}{dt} = f_{i-1} c_{i-1} c - f_i c_i c + b_{i+1} c_{i+1} - b_i c_i + s_i F - l_i c_i F,$$

for $2 \leq i \leq k-1$.

The change in the c_k species, the nucleus in this model, and fibril end populations are

$$\frac{dc_k}{dt} = f_{k-1} c_{k-1} c - f_k c_k c + b_{k+1} F - b_k c_k + s_k F - l_k c_k F,$$

and

$$\frac{dF}{dt} = f_k c_k c - b_{k+1} F.$$

Furthermore, we keep track of the mass of monomers in fibrils over time as well. The resulting equation for monomer mass in fibrils is given by

$$\frac{dM}{dt} = f_{k+1}cF + \sum_{j=1}^{k} l_j c_j F - \sum_{j=0}^{k} s_j F - b_{k+1}F.$$

Here, again, we are tracking fibril density F as opposed to stable nuclei ν, as no stable nuclei are assumed in this model.
To determine whether our data would support this mechanism, we introduce the following scaling variables,

$$\hat{t} = \frac{t}{\lambda c_o^{-\gamma}}, \qquad \hat{c} = \frac{c}{c_o},$$
$$\hat{c}_i = \frac{c_i}{X}, \qquad \text{for } 2 \leq i \leq k,$$

where λ is needed to keep the units correct, and X is a quantity to be determined by the system. Likewise,

$$\hat{F} = \frac{F}{\mu}, \quad \text{and} \quad \hat{M} = \frac{M}{c_o},$$

where μ is a quantity to be determined by the system. Substituting the above into the model and dropping the $\hat{}$s gives

$$\frac{dc}{dt} = \frac{\lambda c_o^{-\gamma}}{c_o}[-f_{k+1}cc_oF\mu + s_oF\mu],$$
$$\frac{dc_1}{dt} = \frac{\lambda c_o^{-\gamma}}{X}[f_0c^2c_o^2 - f_1c_1Xcc_o + b_2c_2X - b_1c_1X + s_1F\mu - l_1c_1XF\mu],$$
$$\frac{dc_i}{dt} = \frac{\lambda c_o^{-\gamma}}{X}[f_{i-1}c_{i-1}Xcc_o - f_ic_iXcc_o + b_{i+1}c_{i+1}X - b_ic_iX + s_iF\mu - l_ic_iXF\mu] \quad \text{for } 2 \leq i \leq k-1.$$

Furthermore, we have

$$\frac{dc_k}{dt} = \frac{\lambda c_o^{-\gamma}}{X}[f_{k-1}c_{k-1}Xcc_o - f_kc_kXcc_o + b_{k+1}F\mu - b_kc_kX + s_kF\mu - l_kc_kXF\mu],$$

and

$$\frac{dF}{dt} = \frac{\lambda c_o^{-\gamma}}{\mu}[f_kc_kXcc_o - b_{k+1}F\mu].$$

The mass of monomer in fibrisl is

$$\frac{dM}{dt} = \frac{\lambda c_o^{-\gamma}}{c_o}[f_{k+1} c c_o F\mu + \sum_{j=1}^{k} l_j c_j X F\mu - \sum_{j=0}^{k} s_j F\mu - b_{k+1} F\mu].$$

We now attempt to remove all explicit dependence of the model on c_o. Inspection of the equations for the change in fibril end density and mass imply that the term $f_k c_k X c c_o$ must survive or no fibrils will ever form. Therefore, we set

$$X = c_o^{\gamma}, \quad \text{and} \quad \mu = X.$$

The resulting equations are

$$\frac{dM}{dt} = \lambda[f_{k+1} c F + \sum_{j=1}^{k} l_j c_j F c_o^{\gamma-1} - s_k F c_o^{-\gamma} - b_{k+1} F c_o^{-\gamma}],$$

and

$$\frac{dF}{dt} = \lambda[f_k c_k c c_o^{-\gamma+1} - b_{k+1} F c_o^{-\gamma}].$$

The equation for the c_k species becomes

$$\frac{dc_k}{dt} = \lambda[f_{k-1} c_{k-1} c c_o^{-\gamma+1} - f_k c_k c c_o^{-\gamma+1} + b_{k+1} F c_o^{-\gamma} - b_k c_k c_o^{-\gamma} + s_k F c_o^{-\gamma} - l_k c_k F c_o^{-\gamma+1}].$$

Furthermore,

$$\frac{dc_i}{dt} = \lambda[f_{i-1} c_{i-1} c c_o^{-\gamma+1} - f_i c_i c c_o^{-\gamma+1} + b_{i+1} c_{i+1} c_o^{-\gamma} - b_i c_i c_o^{-\gamma} + s_i F c_o^{-\gamma} - l_i c_i F],$$
for $2 \leq i \leq k-1$,

$$\frac{dc_1}{dt} = \lambda[f_0 c^2 c_o^{-2\gamma+2} - f_1 c_1 c c_o^{-\gamma+1} + b_2 c_2 c_o^{\gamma} - b_1 c_1 c_o^{-\gamma} + s_1 F c_o^{-\gamma} - l_1 c_1 F],$$

and,

$$\frac{dc}{dt} = \lambda[-f_{k+1} c F + s_o c_o^{-1} F].$$

We now set $\gamma = 1$ and absorb λ into the reaction rates. Our model reduces to

$$\frac{dc}{dt} = -f_{k+1} c F,$$

$$\frac{dc_1}{dt} = f_0 c^2 - f_1 c c_1 - l_1 c_1 F,$$

$$\frac{dc_i}{dt} = f_{i-1} c c_{i-1} - f_i c c_i - l_i c_i F,$$

$$\frac{dc_k}{dt} = f_k c_{k-1} c - f_k c_k c - l_k c_k F,$$

$$\frac{dF}{dt} = f_{k-1} c_k c,$$

and

$$\frac{dM}{dt} = f_{k+1} c_k c + \sum_{j=1}^{k} l_j c_j F.$$

However, elongation kinetics suggest that fibrills grow by monomer addition resulting in

$$\sum_{j=1}^{k} l_j c_j F = 0.$$

Modifying the above model by allowing oligomers to grow by the addition of any number of monomers at each step and following the scaling procedure results in the NDP model. Thus, no new dynamics or insight have been elucidated with this model. Furthermore, given our data, the model is less general than the basic nucleation dependent model.

11.4 Scaling of the Nucleated Polymerization Model with Competing Off-Pathway Aggregation

Here we write the model proposed by Powers and Powers (30) in the notation of this thesis. The assumptions made for the basic NDP model apply here. However, Powers and Powers have imposed the artificial scaling,

$$t_0 \propto A_\infty^{-\gamma}, \qquad \text{for } \gamma = 1.$$

A stated in Section [6.3], the model allows nuclei to form through the addition of one monomer at a time to the preceding oligomeric species and fibril elongation by monomer addition. These definitions, and the diagram shown in Figure(14) result in the following system of differential equations for nucleated polymerization. For the oligomeric and aggregate species we have

$$\frac{dc_1}{dt} = f_0 c^2 - f_1 c c_1 + b_2 c_2 - b_1 c_1,$$
$$\frac{dc_i}{dt} = f_{i-1} c c_{i-1} - f_i c c_i - b_i c_i + b_{i+1} c_{i+1}, \qquad \text{for } 2 \leq i \leq k,$$
$$\frac{dz_1}{dt} = \alpha_0 c^2 - \alpha_1 z_1 c + \beta_2 z_2 - \beta_1 z_1,$$
$$\frac{dz_i}{dt} = \alpha_{i-1} z_{i-1} c - \alpha_i z_i c - \beta_i z_i + \beta_{i+1} z_{i+1}, \qquad \text{for } 2 \leq i \leq m-1,$$

and the change in the largest aggregate species allowed is given by

$$\frac{dz_m}{dt} = \alpha_{m-1} z_{m-1} c - \beta_m z_m.$$

We also obtain,

$$\frac{d\nu}{dt} = f_k c^{n_k} c_k - b_\nu \nu.$$

Furthermore, the total mass of monomers in fibril form, discounting the monomer in oligomer, aggregate and nuclei, is given by,

$$\frac{dM}{dt} = f_{k+1} c \nu - b_M \nu.$$

We now introduce the scaling variables of section [6.3]. Substituting into the model and dropping the $\hat{}$s gives the following equations for the change in the c_1 and z_1 species

$$\frac{dc_1}{dt} = \frac{\lambda c_o^{-\gamma}}{X}[f_0 c^2 c_o^2 - f_1 c_1 X c c_o + b_2 c_2 X - b_1 c_1 X],$$

and

$$\frac{dz_1}{dt} = \frac{\lambda c_o^{-\gamma}}{Y}[\alpha_0 c^2 c_o - \alpha_1 z_1 Y c c_o + \beta_2 z_2 Y - \beta_1 z_1 Y].$$

For the ith species

$$\frac{dc_i}{dt} = \frac{\lambda c_o^{-\gamma}}{X}[f_{i-1} c_{i-1} X c c_o - f_i c_i X c c_o - b_i c_i X + b_{i+1} c_{i+1} X], \quad \text{for } 2 \leq i \leq k,$$

and

$$\frac{dz_i}{dt} = \frac{\lambda c_o^{-\gamma}}{Y}[\alpha_{i-1} z_{i-1} Y c c_o - \alpha_i z_i Y c c_o - \beta_i z_i Y + \beta_{i+1} z_{i+1} Y], \quad \text{for } 2 \leq i \leq m-1.$$

The mth aggregate rate of change is now

$$\frac{dz_m}{dt} = \frac{\lambda c_o^{-\gamma}}{Y}[\alpha_{m-1} z_{m-1} Y c c_o - \beta_m z_m Y].$$

The nuclei and fibril mass rate of changes are

$$\frac{d\nu}{dt} = \frac{\lambda c_o^{-\gamma}}{\mu}[f_k c_k X c c_o - b_\nu \nu \mu],$$

and

$$\frac{dM}{dt} = \frac{\lambda c_o^{-\gamma}}{c_o}[f_{k+1} \nu \mu c c_o - b_M \nu \mu].$$

We now let $\mu = X = c_o^\gamma$. The fibril mass and nuclei concentration rates of change now become

$$\frac{dM}{dt} = \lambda[f_{k+1} \nu c - b_M \nu c_o^{-1}],$$

and

$$\frac{d\nu}{dt} = \lambda[f_k c_k c c_o^{-\gamma+1} - b_\nu \nu c_o^{-\gamma}].$$

The equations for the c_is are

$$\frac{dc_i}{dt} = \lambda[f_{i-1}c_{i-1}cc_o^{-\gamma+1} - f_i c_i c c_o^{-\gamma+1} - b_i c_i c_o^{-\gamma} + b_{i+1}c_{i+1}c_o^{-\gamma}], \quad \text{for } 2 \leq i \leq k.$$

We now write the equation for c_1

$$\frac{dc_1}{dt} = \lambda[f_0 c^2 c_o^{-2\gamma+2} - f_1 c_1 c c_o^{-\gamma+1} + b_2 c_2 c_o^{-\gamma} - b_1 c_1 c_o^{-\gamma}].$$

and,

We are now in a position to impose the only scaling of γ that will allow oligomers and nuclei to form in this model. Specifically, $\gamma = 1$. Furthermore to allow off-pathway aggregates to form we require, $Y = c^\gamma$. This results in the above equations simplifying to

$$\frac{dc_1}{dt} = \lambda[f_0 c^2 - f_1 c_1 c],$$

$$\frac{dc_i}{dt} = \lambda[f_{i-1}c_{i-1}c - f_i c_i c c], \quad \text{for } 2 \leq i \leq k,$$

$$\frac{d\nu}{dt} = \lambda[f_k c_k c],$$

and

$$\frac{dM}{dt} = \lambda[f_{k+1}\nu c].$$

Furthermore, the rates of change for the off-pathway aggregates become

$$\frac{dz_1}{dt} = \lambda[\alpha_0 c^2 - \alpha_1 z_1 c],$$

$$\frac{dz_i}{dt} = \lambda[\alpha_{i-1}z_{i-1}c - \alpha_i z_i c], \quad \text{for } 2 \leq i \leq m-1.$$

The change in the largest aggregate, in monomer units, is now given by

$$\frac{dz_m}{dt} = \lambda[\alpha_{m-1}z_{m-1}c].$$

Therefore, we see that scaling restricts off-pathway kinetics of aggregate formation, as well as, on-pathway kinetics for oligomer formation. Furthermore the aggregate population will only grow while monomers are present and not act as an equilibrium "buffer". Thus, the rate of monomer in fibril should continue to scale even with high initial monomer concentrations as is observed for hIAPP. We now relax the implicit power law with $\gamma = -1$ and rewrite the model in a more generic form so as to let our data motivate the power law used.

11.5 Scaling of the Generic Nucleated Polymerization Model with Competing Off-Pathway Aggregation

We now rewrite the nucleation dependent polymerization model with off-pathway aggregates where oligomers and aggregates are allowed to form by any number of monomers joining to form the first species. Subsequent species are allowed to form by binding to any number of monomers to form the next largest species. No constraint is imposed that requires oligomers and aggregates to be made of the same number of monomer units. However, aggregates may only form from monomers or other aggregates, likewise oligomers may only form from monomers and other oligomers. The definitions of Section [6.4], and the diagram shown in Figure(15) result in the following system of differential equations for nucleated polymerization.

$$\frac{dc_1}{dt} = f_0 c^{n_o} - f_1 c_1 c^{n_1} + b_2 c_2 - b_1 c_1,$$

and

$$\frac{dz_1}{dt} = \alpha_0 c^{a_o} - \alpha_1 z_1 c^{a_1} + \beta_2 z_2 - \beta_1 z_1.$$

For the ith aggregate and oligomer we have

$$\frac{dc_i}{dt} = f_{i-1} c_{i-1} c^{n_{i-1}} - f_i c_i c^{n_i} - b_i c_i + b_{i+1} c_{i+1}, \quad \text{for } 2 \leq i \leq k,$$

and

$$\frac{dz_i}{dt} = \alpha_{i-1} z_{i-1} c^{a_{i-1}} - \alpha_i z_i c^{a_i} - \beta_i z_i + \beta_{i+1} z_{i+1}, \quad \text{for } 2 \leq i \leq m-1.$$

The change in the largest aggregate species allowed is now given by

$$\frac{dz_m}{dt} = \alpha_{m-1} z_{m-1} c^{a_{m-1}} - \beta_m z_m.$$

We also obtain

$$\frac{d\nu}{dt} = f_k c^{n_k} c_k - b_\nu \nu.$$

Furthermore, the total mass of monomers in fibril form, discounting the monomer in oligomer, aggregate and nuclei, is given by

$$\frac{dM}{dt} = f_{k+1} c\nu - b_M \nu.$$

We now introduce the scaling variables of Section [6.4]. Substituting into the model

and dropping the $\hat{\text{s}}$ gives the change in the c_1 and z_1 species as

$$\frac{dc_1}{dt} = \frac{\lambda c_o^{-\gamma}}{X}[f_0 c^{n_o} c_o^{n_o} - f_1 c_1 X c^{n_1} c_o^{n_1} + b_2 c_2 X - b_1 c_1 X],$$

and

$$\frac{dz_1}{dt} = \frac{\lambda c_o^{-\gamma}}{Y}[\alpha_0 c^{a_o} c_o^{a_o} - \alpha_1 z_1 Y c^{a_1} c_o^{a_1} + \beta_2 z_2 Y - \beta_1 z_1 Y].$$

For the ith species

$$\frac{dc_i}{dt} = \frac{\lambda c_o^{-\gamma}}{X}[f_{i-1} c_{i-1} X c^{n_{i-1}} c_o^{n_{i-1}} - f_i c_i X c^{n_i} c_o^{n_i} - b_i c_i X + b_{i+1} c_{i+1} X], \quad \text{for } 2 \leq i \leq k,$$

and

$$\frac{dz_i}{dt} = \frac{\lambda c_o^{-\gamma}}{Y}[\alpha_{i-1} z_{i-1} Y c^{a_{i-1}} c_o^{a_{i-1}} - \alpha_i z_i Y c^{a_i} c_o^{a_i} - \beta_i z_i Y + \beta_{i+1} z_{i+1} Y], \quad \text{for } 2 \leq i \leq m-1.$$

The mth aggregate rate of change is now

$$\frac{dz_m}{dt} = \frac{\lambda c_o^{-\gamma}}{Y}[\alpha_{m-1} z_{m-1} Y c^{a_{m-1}} c_o^{a_{m-1}} - \beta_m z_m Y].$$

The nuclei and fibril mass rate of changes are

$$\frac{d\nu}{dt} = \frac{\lambda c_o^{-\gamma}}{\mu}[f_k c_k X c^{n_k} c_o^{n_k} - b_\nu \nu \mu],$$

and

$$\frac{dM}{dt} = \frac{\lambda c_o^{-\gamma}}{c_o}[f_{k+1} \nu \mu c c_o - b_M \nu \mu].$$

We now let

$$\mu = c_o^\gamma = X.$$

The fibril mass and nuclei concentration rates of change now become

$$\frac{dM}{dt} = \lambda[f_{k+1} \nu c - b_M \nu c_o^{-1}],$$

and

$$\frac{d\nu}{dt} = \lambda[f_k c_k c^{n_k} c_o^{-\gamma+n_k} - b_\nu \nu c_o^{-\gamma}].$$

The equations for the c_is are

$$\frac{dc_i}{dt} = \lambda[f_{i-1}c_{i-1}c^{n_{i-1}}c_o^{-\gamma+n_{i-1}} - f_i c_i c^{n_i} c_o^{-\gamma+n_i} - b_i c_i c_o^{-\gamma} + b_{i+1}c_{i+1}c_o^{-\gamma}], \quad \text{for } 2 \leq i \leq k.$$

We now write the equation for c_1

$$\frac{dc_1}{dt} = \lambda[f_0 c^{n_o} c_o^{-2\gamma+n_o} - f_1 c_1 c^{n_1} c_o^{-\gamma+n_1} + b_2 c_2 c_o^{-\gamma} - b_1 c_1 c_o^{-\gamma}].$$

We now set

$$n_i = \gamma \quad \text{for} \quad i \leq 1 \leq k,$$

and

$$n_o = 2\gamma,$$

reducing the equations for oligomers, nuclei and fibril mass to

$$\frac{dc_1}{dt} = \lambda[f_0 c^{2\gamma} - f_1 c_1 c^{\gamma}],$$

$$\frac{dc_i}{dt} = \lambda[f_{i-1}c_{i-1}c^{\gamma} - f_i c_i c^{\gamma}], \quad \text{for } 2 \leq i \leq k,$$

$$\frac{d\nu}{dt} = \lambda[f_k c_k c^{\gamma}],$$

and

$$\frac{dM}{dt} = \lambda[f_{k+1}\nu c].$$

Furthermore, the equations for off-pathway aggregates are now given by

$$\frac{dz_i}{dt} = \lambda[\alpha_{i-1}z_{i-1}c^{a_{i-1}}c_o^{-\gamma+a_{i-1}} - \alpha_i z_i c^{a_i} c_o^{-\gamma+a_i} - b_i z_i c_o^{-\gamma} + \beta_{i+1}z_{i+1}c_o^{-\gamma}], \quad \text{for } 2 \leq i \leq k.$$

and

$$\frac{dz_1}{dt} = \lambda[\alpha_0 c^{a_o} c_o^{-\gamma+a_o} Y^{-1} - \alpha_1 c_1 c^{a_1} c_o^{-\gamma+a_1} + \beta_2 z_2 c_o^{-\gamma} - \beta_1 z_1 c_o^{-\gamma}],$$

We now set

$$a_i = \gamma \quad \text{for} \quad 1 \leq i \leq m,$$

and remove the explicit dependance on c_o by setting terms explicitly containing c_o to 0. The resulting equations are,

$$\frac{dz_1}{dt} = \lambda[\alpha_0 c^{a_o} c_o^{-\gamma+a_o} Y^{-1} - \alpha_1 z_1 c^{\gamma}],$$

$$\frac{dz_i}{dt} = \lambda[\alpha_{i-1} z_{i-1} c^{\gamma} - \alpha_i z_i c^{\gamma}], \quad \text{for } 2 \leq i \leq m-1.$$

The change in the largest aggregate is now given by

$$\frac{dz_m}{dt} = \lambda[\alpha_{m-1} z_{m-1} c^{\gamma}].$$

We now set $Y = c^{-\omega}$. The resulting equation for $\frac{dz_1}{dt}$ is given by

$$\frac{dz_1}{dt} = \lambda[\alpha_0 c^{a_o} c_o^{-\gamma-\omega+a_o} - \alpha_1 z_1 c^{\gamma}].$$

Thus, we are left with the result

$$a_o = \gamma + \omega,$$

while the solution

$$a_o = 2\gamma,$$

implying

$$\gamma = \omega$$

is possible, it is not a unique solution and we are left with an uncertainty in a_o. Therefore, our equation for $\frac{dz_1}{dt}$ may only be reduced to

$$\frac{dz_1}{dt} = \lambda[\alpha_0 c^{a_o} - \alpha_1 z_1 c^{\gamma}],$$

where

$$a_o = \gamma + \omega.$$